Mudbanks on the Guianas coast

Using satellite images to study the spatial distribution of mudbanks

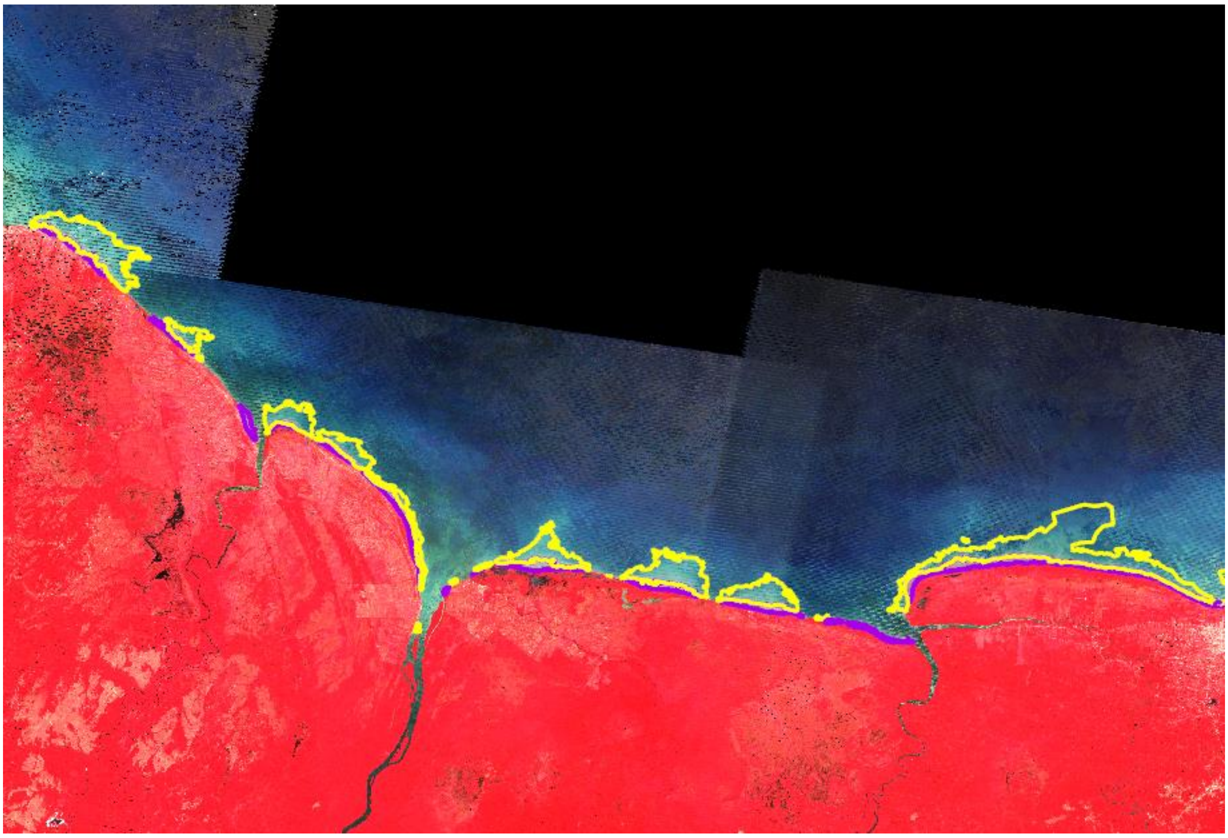

Bachelor's Thesis: Kim de Wit

Student nr: 5636701

Supervisors: dr. Wiebe Nijland and prof. dr. Steven de Jong

Utrecht University, Faculty of Geosciences, 2018

Abstract

The Guiana Coast in South-America is the world's largest mud coast. This area between the Amazon and Orinoco rivers receives great amounts of fine sediment from the Amazon river that is deflected in a north-westward direction along the coast by the Guiana Current. This results in the forming of mudbanks that are important for the dynamics of the coast. In areas were mudbanks lie in front of the coast the area is protected from wave action and accumulation can take place. In the area between the banks the coast is susceptible for erosion. The mudbanks are constantly migrating along the coast, causing the areas of erosion or accumulation to move as well. The coastal area, up to 77 km land inwards, is home to ninety five percent of the inhabitants of these countries that are influenced by changes to the coast. The mudbanks and the coast have been extensively studied, but there still remain many unknowns. For example, how will global climate change and subsequent sea-level rise in the area, influence the mudbank dynamics? And what are the other main factors that play a role in the distribution and form of the mudbanks? In this study 34 years of satellite images, from the Landsat 4, 5, 7 and 8 satellites from 1984 till 2017, were analysed by using Google Earth Engine and ArcGIS Pro to identify patterns in the mudbank dynamics. A CART classification was used to classify the images using the four classes land, water, intertidal mudbank and subtidal mudbank. This classification method has an accuracy of approximately 83-87 %. The classification images were exported to ArcGIS Pro to enhance and analyse them. The classifications were placed as outlines over the original Landsat images to show how the classification data correlates with the real situation. The images were compared for each year, looking at the locations, size, form and amount of mudbanks. Different patterns in the changes of the mudbanks were identified. The bank size and form differ from year to year, with some banks eroding while others are growing due to the redistribution of the sediment. Some changes can be linked to high wave or storm events, such as the decrease in size in 2005, which happened after a high wave event had occurred. Phases of erosion and accretion of the banks are also linked to the direction and strength of the trade winds. Beside natural fluctuations, human activity plays an important role in the bank dynamics as well. The removing of mangrove forests for economic profits can reduce the bank strength which will result in more erosion.

Key words: Mudbank, trade wind, satellite image, CART classification, Guianas

Contents

1. Introduction

The Amapa-Guianas coast is the world's longest mud coast. The area is part of the northeast coastline of the South American continent. It is shared by five countries, Brazil, French Guiana, Surinam, Guyana and Venezuela (Figure 1). This coastal region forms a highly dynamic sedimentary environment as it lies downdrift of the Amazon river and therefore receives large sediment inputs (Allison et al. 2000). Along a length of approximately 1400 km mudbanks can be found, between the mouth of the Amazon river in Brazil and the Orinoco river in Venezuela (M.A. Allison, Nittrouer, and Faria 1995). The oblique wave approach causes these mudbanks to move northwestward, away from the Amazon (Fig. 2) (Allison et al. 2000).

Ninety percent of Guyana's population lives in the coastal region, an area of approximately 435 km long and with a width between 77 km in the west and 26 km in the east. This area lies nearly 2.4 m below mean sea level, and with expected sea level rise due to climate change, flooding event will occur more frequently (Ahmad and Lakhan 2012). The consequences of coastal erosion will affect many people who live in the area (Lakhan 1994). Where no mudbank is present, the coast is vulnerable to erosion and settlements on mudflats are lost (Ahmad and Lakhan 2012).

The coastal dynamics are strongly influenced by the presence or absence of mudbanks. Accretion takes place in areas with a mudbank in front of the coast, whereas erosion occurs in the intervals between two mudbanks. If mudbanks remain stationary for a longer period, broad mudflats can develop on the landward side of the coast (Ahmad and Lakhan 2012), on which commonly mangrove forests will develop (Plaziat and Augustinus 2004).

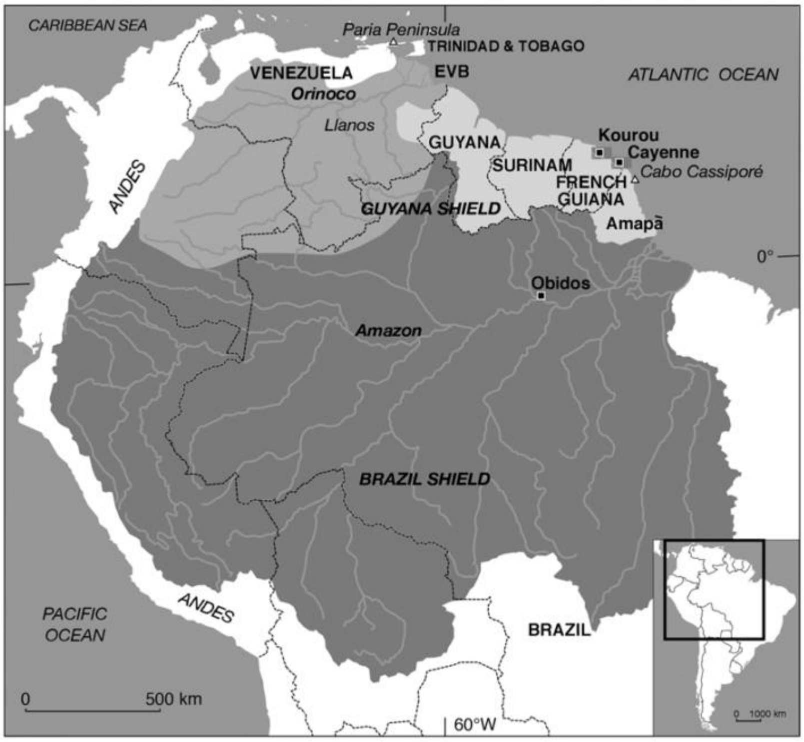

Figure 1. Map showing the Amazon–Orinoco (A–O) coast, and, in three shades of grey, the drainage basins of the Amazon, the Orinoco rivers and, collectively, the smaller Guiana Shield rivers between Amapa, in Brazil, and Guyana. EVB, Eastern Venezuelan Basin (Anthony, Gardel, and Gratiot 2014)

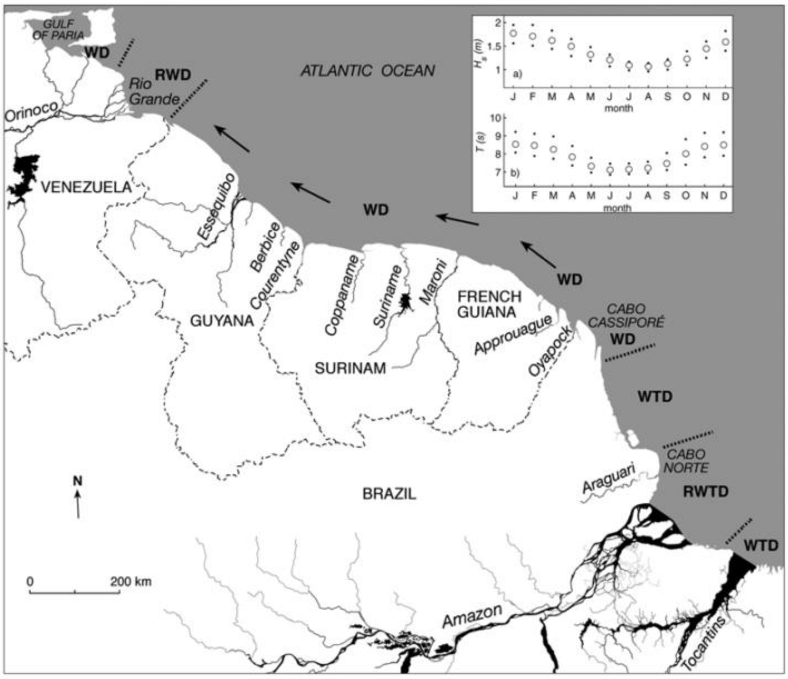

Figure 2. Close-up of the Amapa-Guiana coastline. The arrows show the mudbank migration caused by the longshore waves. An indication is given of whether or not an area is river (R), wave (W) or tidal (T) dominated (D). Some areas are a influenced by a combination of factors (Anthony et al. 2014).

1.1 Formation of the mudbanks

The mudbanks originate in the region of the Cassipore mudcape (Allison et al. 2000). Mudcapes are spit-like features. Their morphology is similar to sand spits, but they are formed in a different way. They are made due to rapid accumulation of mud and as they form on the updrift side of river mouth estuaries, they result in a deflection of the river mouth further downdrift. Mudcapes can be up to 100 km long and 5-10 km wide (Allison et al. 2000; M. A. Allison, Nittrouer, and Kineke 1995). The Cassipore mudcape is located on the northern side of the Amazon river mouth.

In this area on the northern Amapa coast Amazon mud accumulates and from there new mudbanks start to migrate along the coast with rates of 0.5-4.5 km/year. Currently there are approximately 19 mudbanks along the coast, each with space intervals of 15-25 km between them. The timing of the formation of a new mudbank is in the order of 10-20 years (Allison et al. 2000; Anthony et al. 2014). The forming of new mudbanks seems to be related to the strength and direction of the trade winds in this area as the period with which the banks form coincides with coupled atmospheric-oceanographic fluctuations. These fluctuations occur as periods of forcing and relaxation of the North Brazil Current as a result of changes in the wind intensity (Allison et al. 2000; Anthony et al. 2014; Eisma, Augustinus, and Alexander 1991).

The exact processes of the formation of mudbanks is still unknown which is why it is interesting to know the exact timing of the formation of new mudbanks. Also the size of the mudbanks and the speed with which they migrate helps to identify the exact driving forces of the process of mudbank formation. Many researches in this area cover only part of the coastline, but looking at the entire area can show the connections between the different parts which helps identify larger scale trends.

1.2 Satellite images and remote sensing

Remote sensing using satellite images is very useful for identifying trends on the Guiana coastline on a larger scale. Changes to the Guiana Coastline have previously been identified by using maps from the 18th century (Plaziat and Augustinus 2004). More recent studies also used GIS-based analyses for analyzing changes to the coast of Guyana, which proved to an useful method (Ahmad and Lakhan 2012). In this thesis satellite images from the Landsat 4, 5, 7 and 8 satellites were analyzed and classified to map the changes along the coast. The data was obtained by using Google Earth Engine, in which it is possible to create cloudmasks and classifications of images. Other studies show that Google Earth Engine is a powerful tool in classifying satellite images to analyze them for different purposes, such as mapping global surface water, land use mapping of coastal areas or identifying changes in settlement and population over a longer time period (Farda 2017; Patel et al. 2015; Pekel et al. 2016).

The aim of this thesis is to get a clear overview of how mudbanks migrate along the Amapa-Guiana coast.

The research question that is answered in this thesis is: What is the spatial distribution of the mudbanks in front of the coast of the Guianas over the last decennia from 1984 till 2017?

The sub-questions that are answered are:

1. How do the mudbanks change during the research period, in terms of:
    a. Size (their area).
    b. Form
    c. Number of mudbanks: Do any of the mudbanks split up or merge?
2. When did new mudbanks start to form?
3. What is the average speed with which the mudbanks are transported?
4. Where does net erosion or net accumulation take place along the coast during the research period?
5. How are locations of net erosion and net accumulation related to the location of the mudbanks?

The size and distribution of the mudbanks changed significantly in the 34 years analyzed in this thesis. The expectation was that the results show the trends in size, form and splitting or merging of the banks and that these correlate with changes in the trade winds or with other factors such as storm events or human intervention. The different mudbanks were mapped and areas of erosion and accumulation identified to show the exact changes along the coast, which were then compared with the different factors that could play a role in the bank dynamics.

2. Mudbank dynamics

2.1 Mudbank migration

When the sediment has settled in the form of mudbanks it does not rest. Instead the mud is constantly reworked and resuspended due to wave action causing the mudbanks to migrate. On the downstream side of the banks sediment is deposited, while nearly simultaneously on the upstream side the banks are eroded. With the movement of the mudbanks, the interbank areas also move, causing a comigration these areas (Froidefond, Pujos, and Andre 1988; Plaziat and Augustinus 2004).

The three main drivers for mudbank migration are (Froidefond et al. 1988):

1. Waves causing a longshore drift. The waves approach the coast with an angle, causing a longshore drift. Also the fluid muds cause the approaching waves to deform, which could explain a longshore transport.
2. Tidal currents. These currents can influence the migration as they are stronger near river mouths, causing an acceleration of the migration rate. In intertidal zones this has no influence and therefore migration rates are slower.

3. The Guiana Current plays an important role in transporting sediment along the coast. This means it also causes the migration of the mudbanks.

2.2 Morphology of the mudbanks

Mudbanks are up to 5 m thick, 10 to 60 km long and 20 to 30 km wide. Each mudbank may contain approximately the equivalent mass of the annual mud supply of the Amazon River (Anthony et al. 2010).

A mudbank consists of a subtidal and an intertidal part (Figure 3). The upper part of the mudbank is often colonized by a mangrove ecosystem as this part is situated above mean high water level of neap tide. These systems are often dominated by the species Avicennia germinans, which are associated with these conditions (Plaziat and Augustinus 2004).

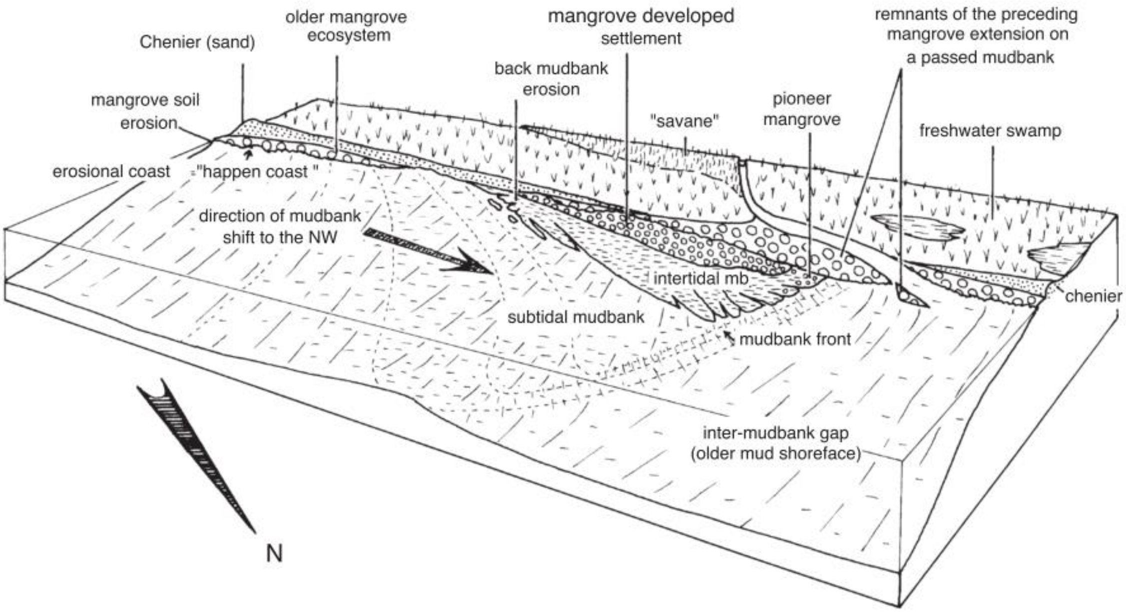

***Figure 3. Block diagram showing a simplified version of the various depositional sub-environments in a shifting mudbank system along the Guiana coast. The morphology of a mudbank is shown with the intertidal and subtidal areas of the mudbank. After* (Plaziat and Augustinus 2004).**

2.3 Influence of mudbanks on the coast

The presence or absence of mudbanks can greatly influence the coastal area. When a mudbank is situated in front of the coast accretion takes place, whilst in the interbank area the coast is eroded (Ahmad and Lakhan 2012; Froidefond et al. 1988; Plaziat and Augustinus 2004).

The mudbank zones are protected from wave attack because the fluid muds dampen the wave energy. This makes the accretion of the coast possible. The accretion is accompanied with rapid mangrove colonization. When the waves are dampened, some of the mud is recycled and individual mud bars will form (Anthony et al. 2010).

When the mudbank passes by and the coast is exposed again in the interbank areas the propagating waves will lead to erosion of the coast. This can cause a muddy shoreline retreat of tens of metres up to several kilometres over a few months to a few years. As the mangrove forests were situated on these mudflats, the erosion will cause a massive loss of mangroves.

3. Methods

Using satellite images the evolution of the mudbanks along the coast was visualized. These satellite images were constructed and processed with Google Earth Engine and with ArcGIS Pro. This section gives a description how the data was constructed and how it was analysed.

3.1 Study area

3.1.1 Oceanographic situation

Different physical oceanographic factors that influence the Guiana coast. Along the north east coast of South America flows the Guiana Current. This current formed as a result of the bifurcation of the North Brazil Current in the North Equatorial Current and the Guiana Current. The North Equatorial current moves in a northeastward direction away from the coast, whilst the Guiana Current moves in a northwestward direction along the coast of the Guianas. The transition between the North Brazil Current and the Guiana current is not a sharp transition but it lies approximately at the mouth of the Amazon River (Bulgakov, Bulgakov, and Eremeev 1998; Metcalf and Stalcup 1967). The Guiana Current flows over the South American continental shelf and is one of the major drivers for sediment transport along the coast (Froidefond et al. 1988). The continental shelf in this area has an average width of 150 km and a slope towards the edge at about 90 to 100 m (Augustinus 1978).

3.1.2 Sediment source/River catchment

The sediment that forms the mudbanks on the coast of the Guianas originates from the Amazon river (Allison et al. 2000). The large mud discharge from the river leads to a fast forming of fluid-mud, which is highly concentrated suspended sediment near the bed. Due to the interaction between the fresh water from the river and the salt water from the ocean the sediment is trapped in a stratified plume (Anthony et al. 2014; Kineke et al. 1996).

Although the large volume of freshwater that comes from the Amazon River causes a salinity anomaly that traps the sediment, the motions are dominated by other factors. Tide-induced mixing has an influence on the position and structure on the bottom salinity front that separates the well-mixed nearshore region from the stratified plume. The plume contains high concentrations of sediment and is moved mostly along-shelf towards the northwest. The velocity with which the plum migrates varies with the wind stress. This causes large temporal variations in the plume structure and freshwater content on the shelf (Rockwell Geyer et al. 1996).

The overall motion of the sediment plume towards the northwest is caused by large scale pressure gradients formed due to the existence of the Guiana Current (Rockwell Geyer et al. 1996).

3.2 Google Earth Engine

For this research the spatial distribution of mudbanks was analysed by using Google Earth Engine. The images that were used are from the Landsat 4, 5 7 and 8 satellites (Table 1). The Landsat satellites have created a large database with a global coverage of images since 1982 with a resolution of 30 m per pixel. The combination of relatively high resolution and a large database makes the Landsat satellite images ideal for analysing the mudbank dynamics on a longer timescale. The data from 1982 and 1983 does not cover the Guianas Coast, therefore the timeseries of this research only covers data from 1984 till 2017.

3.2.1 Landsat datasets

For this research the USGS Landsat 4, 5, 7 and 8 Surface Reflectance Tier 1 datasets were used.

The Landsat 4, 5 and 7 Surface Reflectance Tier 1 datasets contain the atmospherically corrected surface reflectance from their Enhanced Thematic Mapper (ETM) sensors (ETM+ for Landsat 7) (Foga et al. 2017). The images contain 4 visible and near-infrared (VNIR) bands and 2 short-wave infrared

(SWIR) bands processed to orthorectified surface reflectance, and one thermal infrared (TIR) band processed to orthorectified brightness temperature. Only the VNIR bands were, used for this research. They have a resolution of 30 m / pixel (USGS 2017a, 2017b, 2017c).

The data from these three satellites have been corrected using the Landsat Ecosystem Disturbance Adaptive Processing System (LEDAPS) (The Interior Department of USGS 2018a).

The Landsat 8 Surface Reflectance Tier 1 dataset contains the atmospherically corrected surface reflectance from the Landsat 8 Operational Land Imager (OLI)/Thermal Infrared Sensor (TIRS) sensors. The images contain 5 visible and near-infrared (VNIR) bands, which is one more than the Landsat 4, 5 and 7 satellites. It also contains 2 short-wave infrared (SWIR) bands processed to orthorectified surface reflectance, and two thermal infrared (TIR) bands processed to orthorectified brightness temperature (USGS 2017d). From this satellite also only the VNIR bands were used.

The data of the Landsat 8 satellite have been atmospherically corrected using a new system, Landsat 8 Surface Reflectance Code (LaRSC) (The Interior Department of USGS 2018b).

Also a CFMask was added to the four datasets to include a cloud, shadow, water and snow mask, as well as a per-pixel saturation mask. A cloudmask is necessary because in all satellite images clouds are unavoidable, and the best way to create clear pictures is to filter or mask out most of the clouds. An important notion is that CFMask may have difficulties with defining clouds over bright areas such as beaches. Also the efficacy of Surface Reflectance correction will be reduced in for example coastal regions where land area is small relative to adjacent water and areas with extensive cloud contamination. This is because in those areas the atmospheric correction is affected by unfavourable conditions (Foga et al. 2017). Our study area is a coastal area and has much cloud coverage. .This means that creating completely cloud free images is difficult for this are

The World Reference System (WRS) is a global notation used for arranging Landsat data. WRS-2 is used as standard reference grid for the Landsat 4, 5, 7 and 8 data. The collected data strips are placed together into overlapping “scenes” covering approximately 170 km x 183 km following the WRS-2 grid (USGS 2017a, 2017b, 2017c, 2017d, 2018) .

The following bands were used from Landsat 4, 5 and 7: B2, B3, B5 (Table 2). And for Landsat 8 the B3, B4, B5 (Table 3). This combination of bands gives a ‘Color Infrared’ composite that makes the mudbanks better visible, compared to a true color image (Figure 6).

Table 1. Information of the Landsat satellites that were used (Chander, Markham, and Helder 2009; USGS 2017a, 2017b, 2017c, 2017d)

Satellite	Sensors	Launch date	De-commission	Altitude (km)	Inclination (degrees)	Period (min)	Repeat cycle (days)	Crossing time (a.m.)	Nominal resolution (m)
Landsat 4	MSS and TM	July 16, 1982	Dec 14, 1993	705	98.20	98.20	16	9:45	30
Landsat 5	MSS and TM	March 1, 1984	May 5, 2012	705	98.20	98.20	16	9:45	30
Landsat 7	ETM+	April 15, 1999	Operational	705	98.20	98.20	16	10:00	30
EO-1	ALI	November 21, 2000	Operational	705	98.20	98.20	16	10:01	30

Table 2. Details of the used bands Landsat 4, 5, 7 (USGS 2017a, USGS 2017b, USGS 2017c)

Name	Units	Scale	Wavelength	Description
B2		0.0001	0.52-0.60 µm	Band 2 (green) surface reflectance
B3		0.0001	0.63-0.69 µm	Band 3 (red) surface reflectance
B4		0.0001	0.77-0.90 µm	Band 4 (near infrared) surface reflectance

Table 3. Details of the used bands Landsat 8 (USGS 2017d)

Name	Units	Scale	Wavelength	Description
B3		0.0001	0.533-0.590 µm	Band 3 (green) surface reflectance
B4		0.0001	0.636-0.673 µm	Band 4 (red) surface reflectance
B5		0.0001	0.851-0.879 µm	Band 5 (near infrared) surface reflectance

All the data is used in a Google Earth Engine script to create the satellite images that can be used for classification. The complete script can be found in Appendix 1 and here the different steps of the script are briefly discussed. These steps are also schematically visualized in a FlowChart (Figure 4).

3.2.2 Cloudmask

The quality bands of the Landsat images are pixel quality attributes generated from the CFMask algorithm. The pixels that have been assigned to clouds or cloud shadows are masked. The data is also filtered for a maximum cloud coverage of 80 %, so all the image that contain more than 80 % clouds are discarded. The data is also filtered for the area of interest (roi). The quality bands assessment is done separately for the Landsat 4, 5, 7 and Landsat 8 image collections as their bands are different. The selected bands of Landsat 8 are renamed from B3, B4, B5 to B2, B3, B4 to match the bands from the other satellites. Then the image collections from the different satellites are merged into one image collection. The median is taken from this image collection to create an image that can be used for classification.

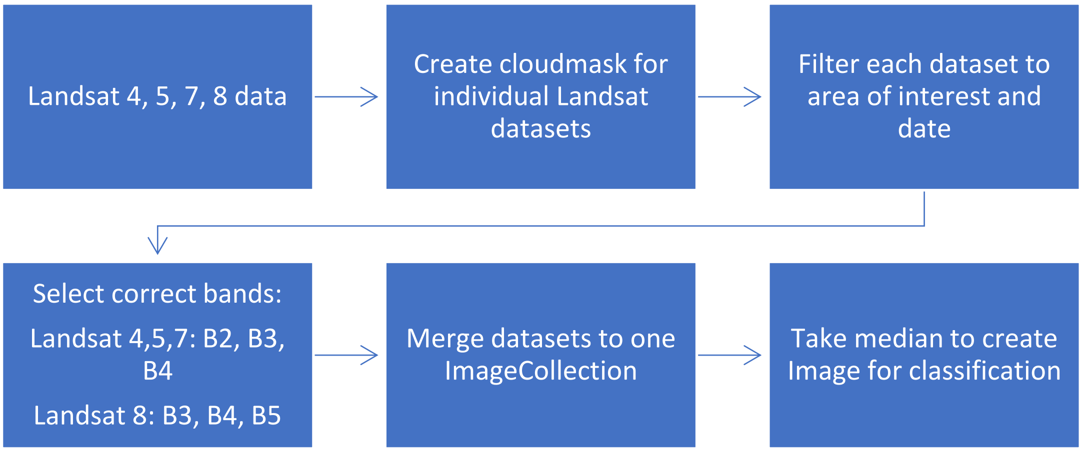

Figure 4. Simplified overview of the process used to create the images for the classification, including cloudmask and data filtering.

3.2.3 Classification

To identify the mudbanks a supervised classification can be used in Earth Engine (Figure 5). This type of classification generates a classification based on the collected training data. The training data exists of a feature collection called "landcover". This feature collection exist of four feature collections, representing the four classes, merged together. The classes that are defined are land, water, intertidal mudbank and subtidal mudbank. Each separate collections contains markers that are placed on the areas of the right landcover type (Figure 6). This tells the classifier which pixels are part of which class. The correct bands are selected to tell the classifier which pixels to select.

With the collected training data a Classification and Regression Trees (CART) classifier is trained (Breiman 1984). This classification methods uses a decision tree to identify to which class a certain training point fits. CART classification is traditionally used in economical but over the past 20 years the method has also been used for ecological problems (Mertens, Nestler, and Huwe 2002). The classification is made for the four classes and it is mapped over the satellite images.

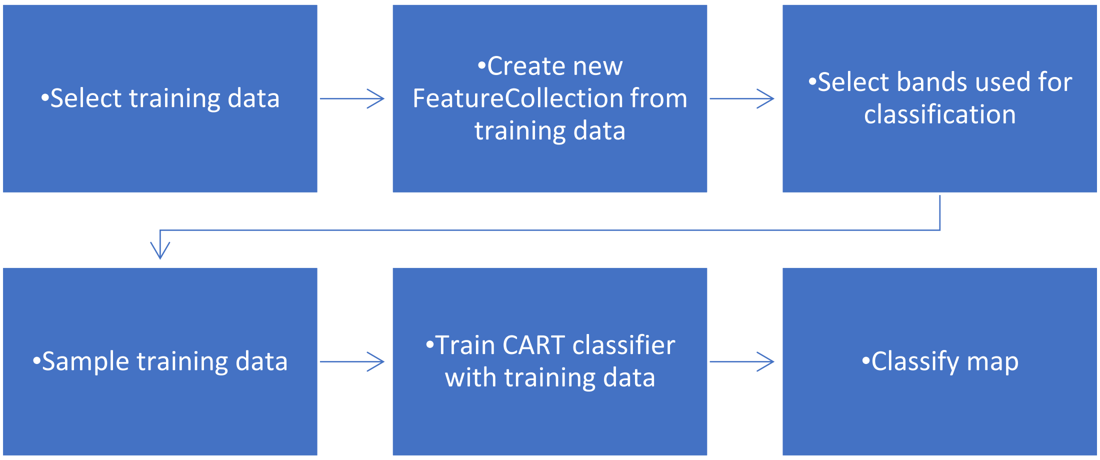

Figure 5. Simplified overview of the classification method.

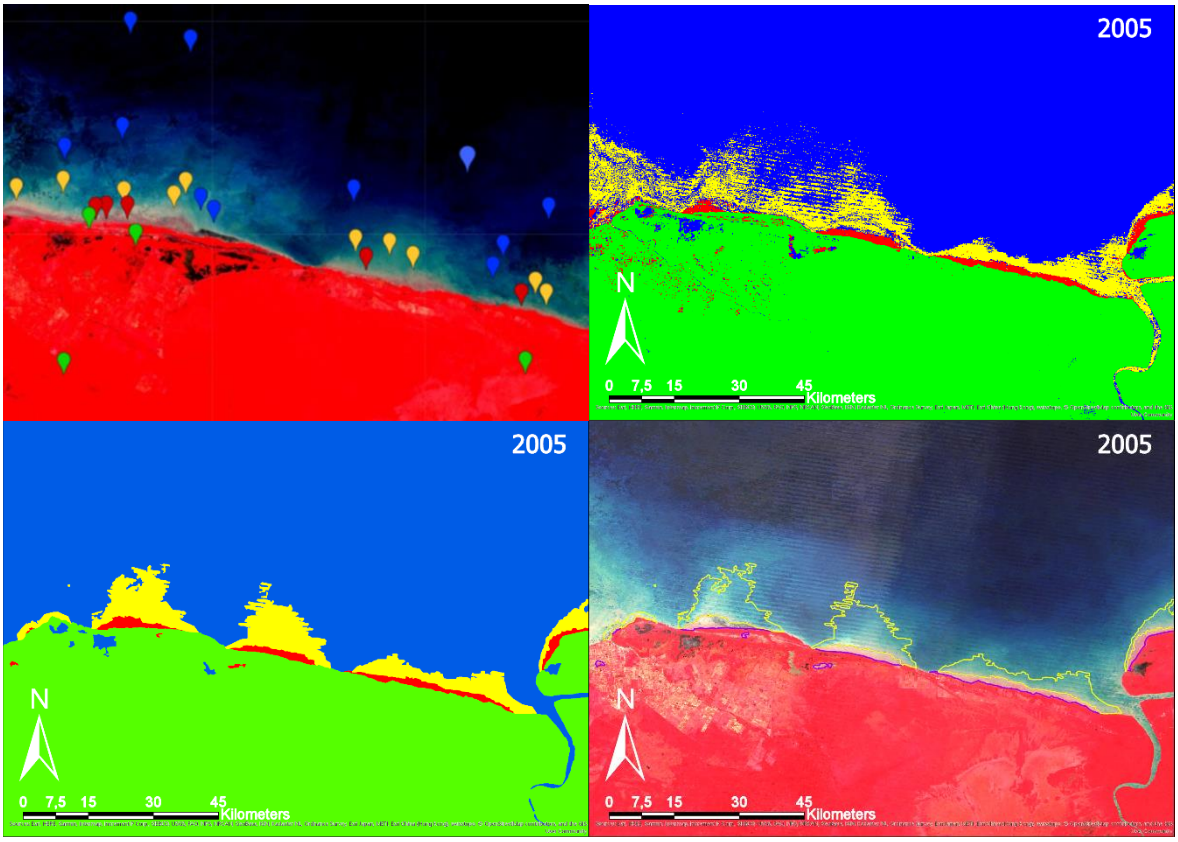

Figure 6. Top left: Landsat image using band B3, B4, and B5 to get a clear image of the mudbanks. Markers for the training data are also shown. Top right: Original classification output placed over the Landsat image. Blue is water, green is land, red is the intertidal mudbank and yellow the subtidal mudbank. Bottom left: Classification after analyses in ArcGIS Pro. Bottom right: Classification outline mapped over original satellite image.

Using this script, separate classification images were constructed for each year from 1999 till 2017. For the period 1984 till 1998 there are less Landsat images available, which makes it hard to construct an useful image of the coast each year. Therefor this period is divided in to three periods of five years of which an image was constructed: 1984-1988, 1989-1993, 1994-1998. These three images and the one from 1999 cover a slightly smaller section of the coastline.

3.2.4 Accuracy assessment

It is important to know how accurate the classification method that is used actually is. Without knowing the error of the classification it is not possible to make concrete conclusions about the data considering you do not know if the changes are due to a measurement error or not. It is possible to assess the accuracy of the classification in Earth Engine, however when this was done an accuracy of 1 was given. This did not seem likely, considering that there were clearly wrong labeled pixels. Looking at several other researches a different accuracies are found for classifications in Earth Engine. A research for mapping land use of coastal regions gave an overall accuracy of 96,98 % for the CART classification they used in Earth Engine (Farda 2017). Another research using Landsat 8 images and a CART classifier in Earth engine shows that the results had an accuracy of 83,1 % to 87,1 %(Goldblatt et al. 2016). An accuracy of 83-87% seems more likely considering there were clearly some wrongly classified pixels.

3.3 ArcGIS Pro

From Google Earth Engine the raster data are saved to Drive as Geotiff files with a resolution of 100m per pixel, using the WGS 84 coordinate system . With this resolution there is still enough detail in the images but the amount of data is slightly reduced to make the dataset more manageable.

The raster data is put into ArcGIS Pro and cleaned up to remove most of the smaller pixels and to construct the individual mudbanks (Figures 6 and 7).

To clean up the images first a majority filter was used to get rid of the smallest pixels. Than the Boundary Clean tool was used to clear the edges of the features. To remove the small pixel clusters the Nibble tool was used. First the different clusters were identified with the Region Group tool. Then all the clusters with less than 100 pixels, which is approximately 1 km^2, were set null with the Set Null tool. A limit of 100 pixels was used to remove unwanted small groups but to make sure small mudbanks were not removed. Finally the Nibble tool is used, using the 'Boundary Clean' layer as input and the 'Set Null' layer as mask.

From the cleaned up images that result from the Nibble tool, editable layers are made with the Raster to Polygon tool. In these layers any excess pixels were removed and all the mudbanks were separated. For each year the area and location of the separate mudbanks was calculated and put in an attribute table.

The polygons of water and land were made invisible, and only the outlines of the mudbanks are shown. These outlines are placed on top of the original satellite image to create a better view of the classification and how it correlates with the actual satellite image (Figure 6).

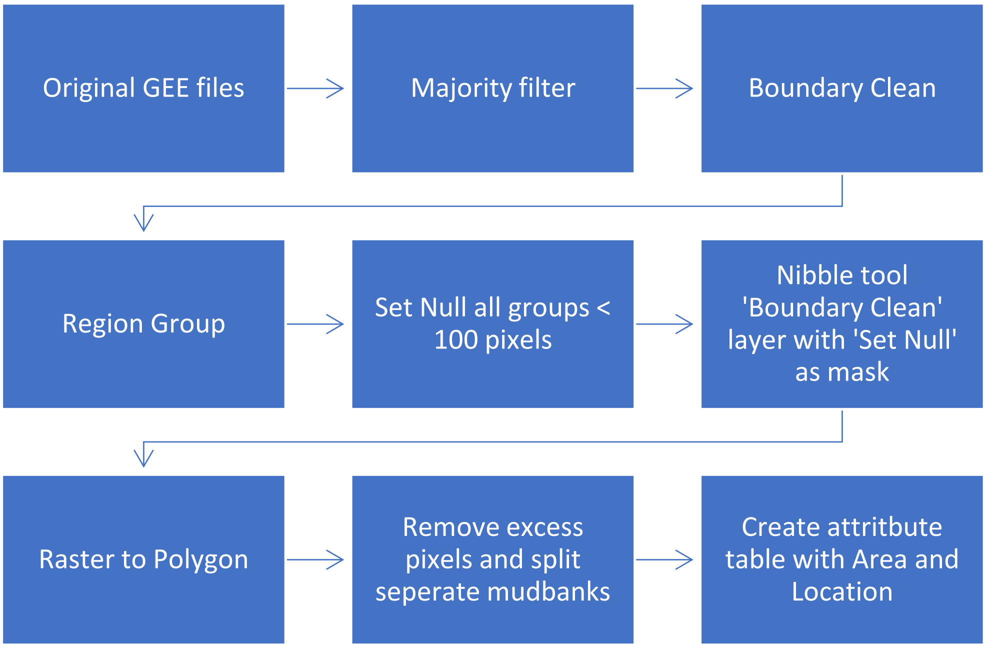

Figure 7. Simplified overview of the analyses in ArcGIS Pro.

4. Results

4.1 Accuracy of the results

The classification of the mudbanks was not flawless, an accuracy of approximately 83-87% was found for the classification method. To minimalize errors in the results and the subsequent conclusions based on these results, the mudbank classifications were placed over the original satellite images

(Figure 6). This shows how well the classifications fit the actual images. For example in section 1 part of the image from 1999 is blurred with black spots. This has caused the classification of bank 1C to be bigger than the actual bank. For the other years the classification fits better over the satellite image. This shows that the accuracy of the classification defers per year and per mudbank, which should be taken into account when looking at the data.

4.2 Analysis of the results

The mudbanks are discussed in this section in groups that are mostly separated by large rivers (Figure 8). For each section the location of the mudbanks is shown on a 6 year interval, so for the years 1999, 2005, 2011 and 2017. For section 3 to 8 image of 1984-1998 were also available. To show the changes of the banks for the other years as well, graphs of the area of the intertidal and subtidal banks are included for each section.

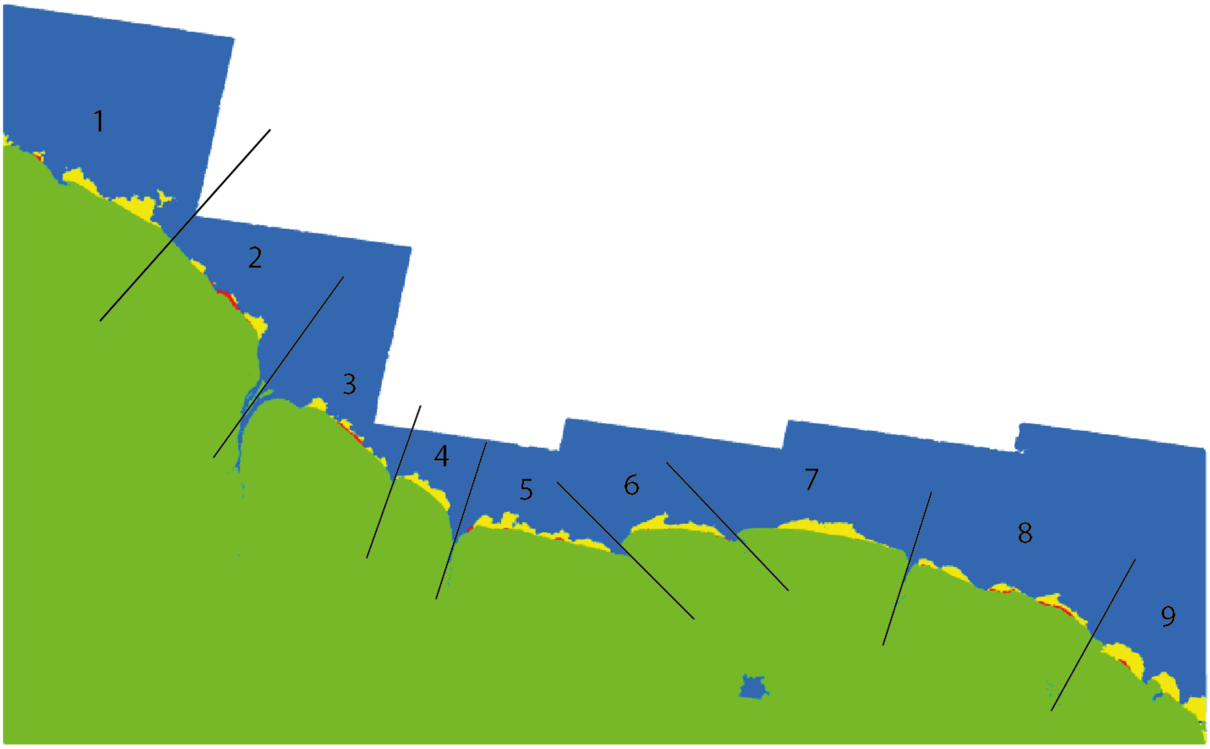

Figure 8. The nine different sections of the research area.

4.2.1 Orinoco River – Halfway to Essequibo river (Figures 9 and 10)

This section has four main mudbanks in 1999, two on the left (A and B) and to on the right (C and D) of the Waini River. Mudbank A and B start of as small separate mudbanks in 1999, but they slowly grow and merge in 2001. Their size fluctuates from 100 up to nearly 500 km^2. The mudbanks are smallest in the years 1999, 2005, 2011, 2012 and 2014. The mudbank stays in approximately the same place during the entire period.

Bank C and D start as large separate mudbanks, but sometimes they merge and then become separate again. Their sizes vary over time with mudbank C becoming drastically smaller, from 200 km^2 1999 to 3 km^2 in 2012. From there it starts growing again and merges with mudbank D in 2017.

The migration of mudbank D is clearly visible. From 2000 to 2017 the center of the bank moved 25,7 km, which is 1,5 km per year.

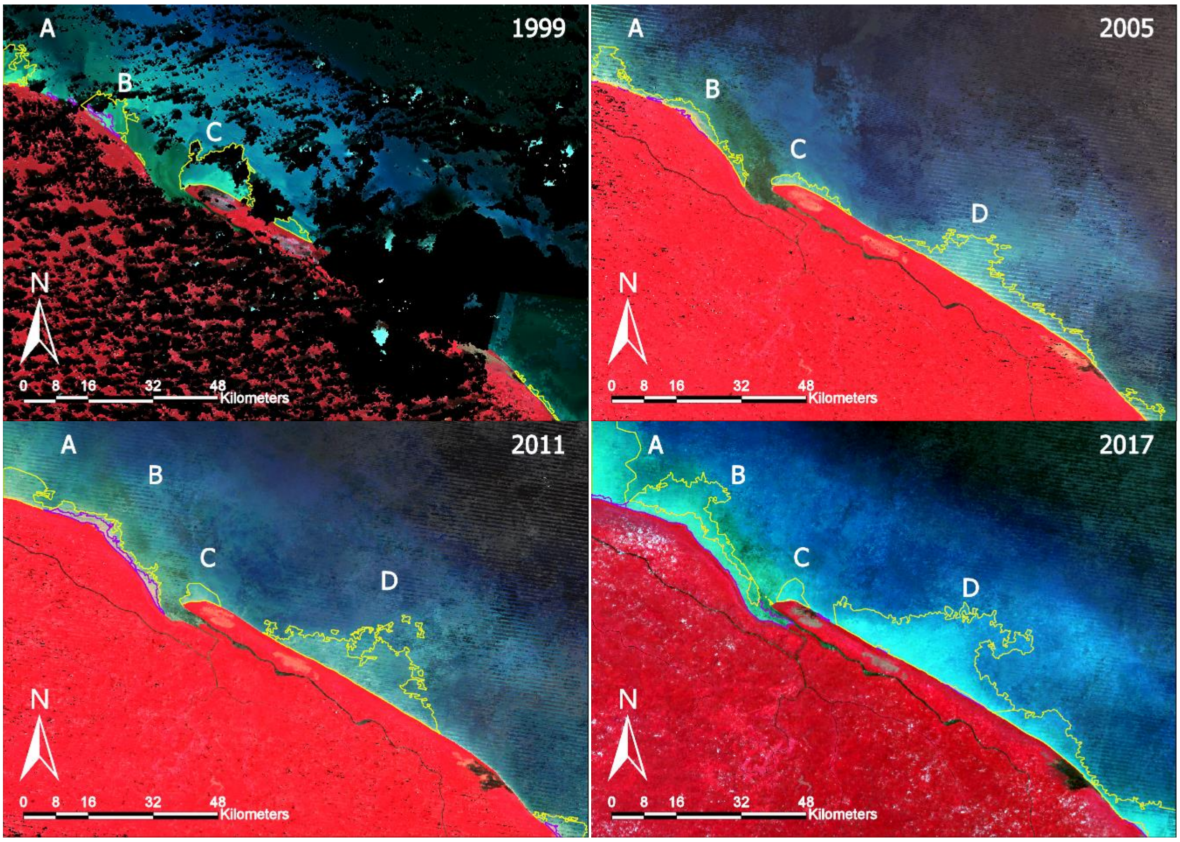

Figure 9. The mudbanks from Section 1 in a selection of the research period. The letters are placed at the right mudbanks for identification.

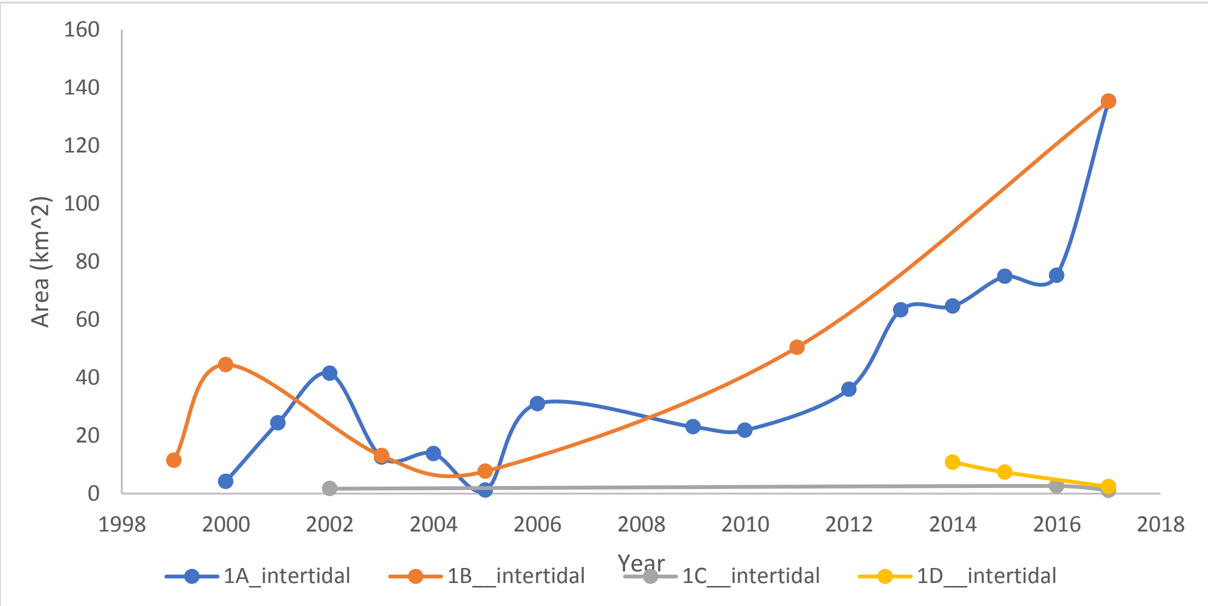

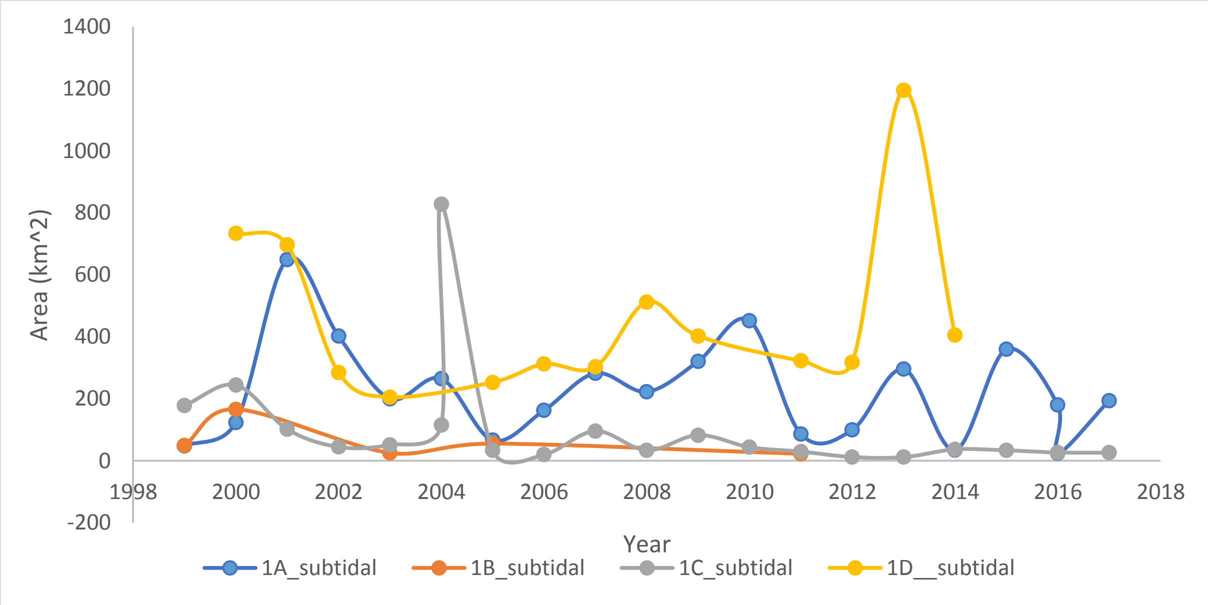

Figure 10. Changes in area of the intertidal (upper graph) and subtidal (lower graph) banks in section 1 from 1998 till 2017.

4.2.2 Halfway to Essequibo river - Essequibo river (Figures 11 and 12)

In 1999 there are 4 mudbanks in this section, but in 2002 A and B have merged. In 2006 a new mudbank (E) exists on the left side of the Essequibo river delta. This bank merges with C in 2007. Then it separates again in 2010 in which the mudbanks are also much smaller. In 2013 the mudbanks grow again, until C and E merge again in 2016.

Bank A also grows during this period but slowly moves away from the other mudbank. However, in 2017 it seems as if the mudbanks have formed one front along the coast but with three separate subtidal parts.

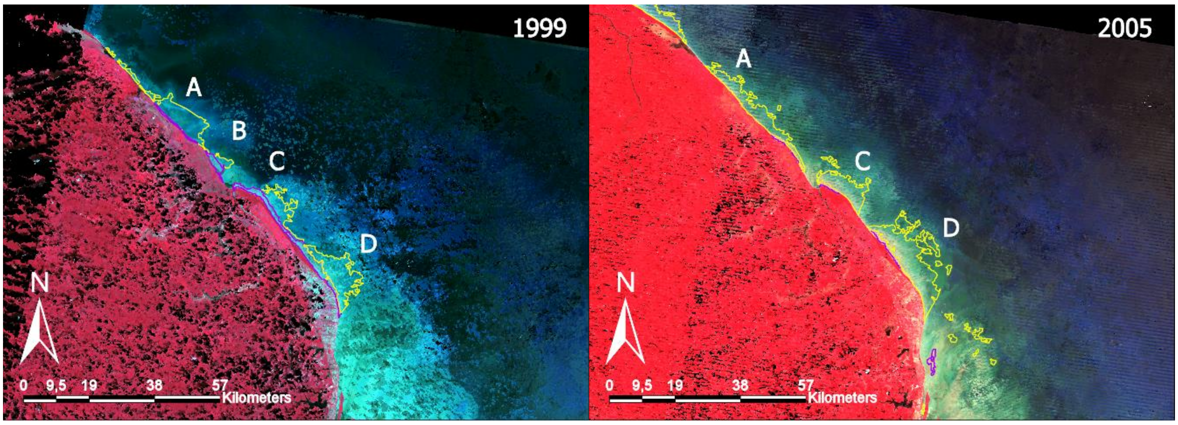

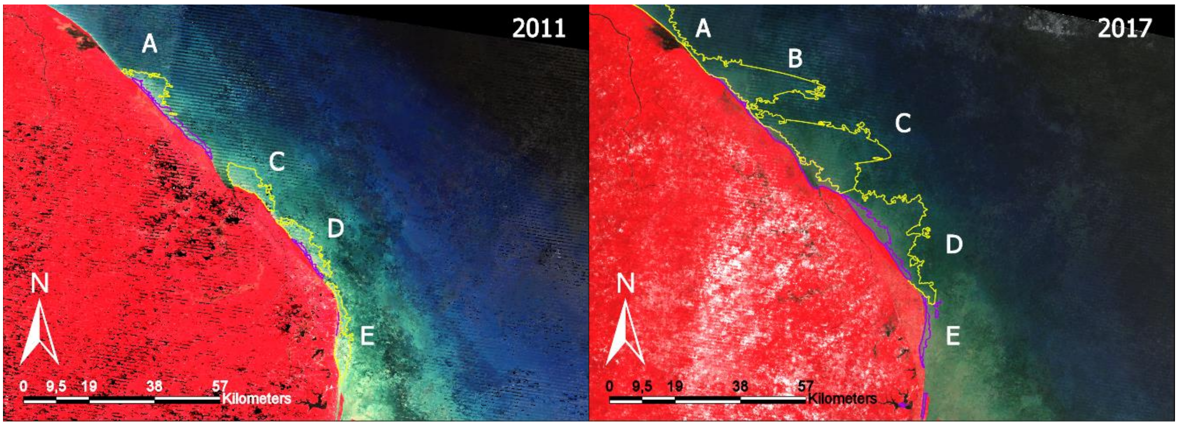

Fig. 11 The mudbanks from Section 2 in a selection of the research period.

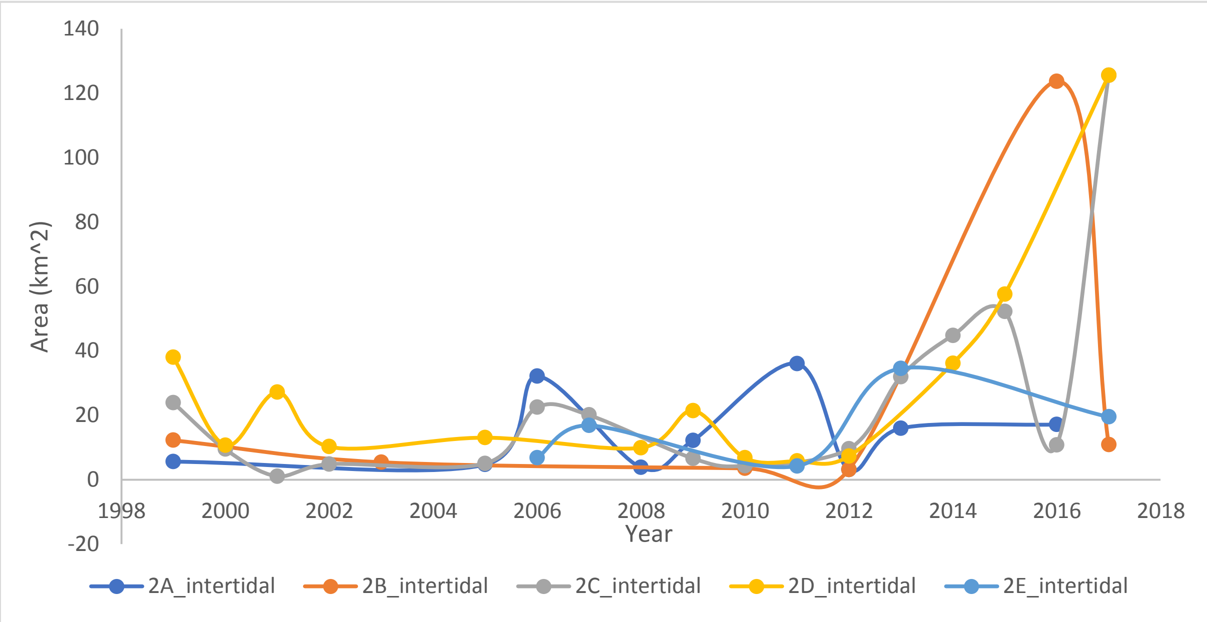

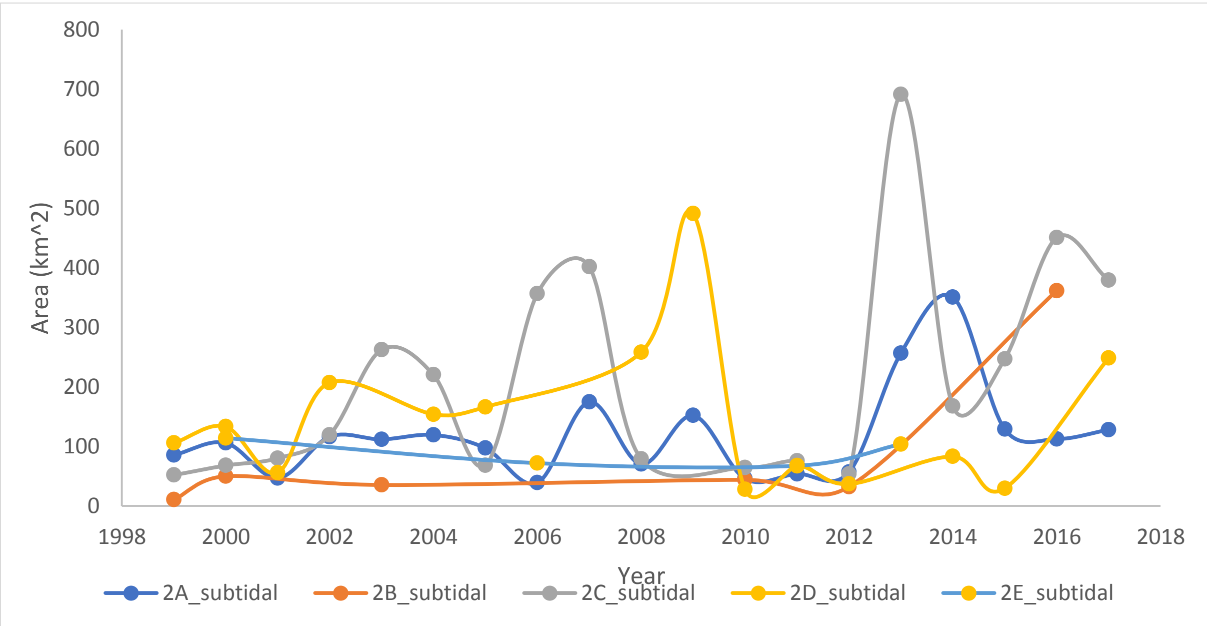

Figure 12. Changes in area of the intertidal (upper graph) and subtidal (lower graph) banks in section 2 from 1998 till 2017.

4.2.3 Essequibo river - Berbice River (Figures 13 and 14)

For this section data from 1984 till 1998 was also available. During this period there was not much change in the form of the mudbanks. There are two mudbanks clearly visible, one of which lies in the delta of the Courantyne River in 1984. Both banks move to the north west and mudbank C clearly moves out of the delta.

From 1999 the west side of this section is also visible and this shows another mudbank near Georgetown. The northwestward movement seems to continue. In 2000 the upper mudbank has split in to two smaller ones, one on each side of the Demerara River. In 2002 mudbank B has merged with A2, but in 2003 A1 and A2 have completely disappeared. In 2005 there appears a new mudbank to the left of the Demerara River, that continues to be there in different sizes till it disappears again in 2017.

In 2006 a new bank appears on the left side of the Courantyne River. It nearly merges with Bank C but bank C becomes smaller till it is only 50 km^2 in 2011. From then it starts to grow again and banks C and D merge in 2013.

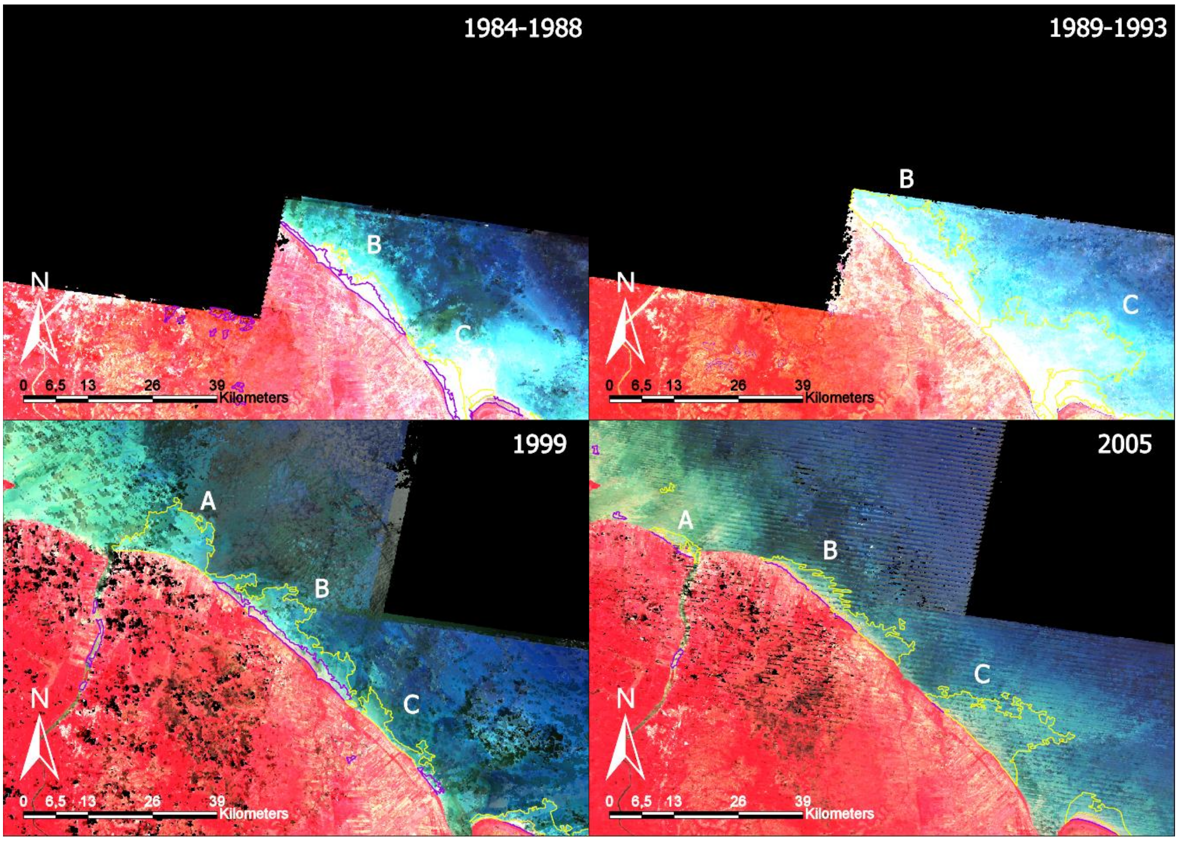

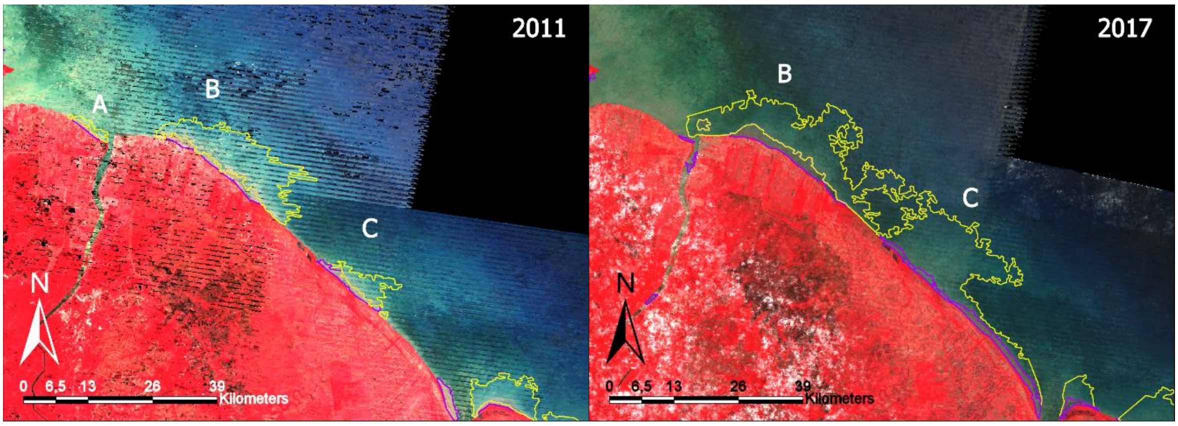

Figure 13. The mudbanks from Section 3 in a selection of the research period.

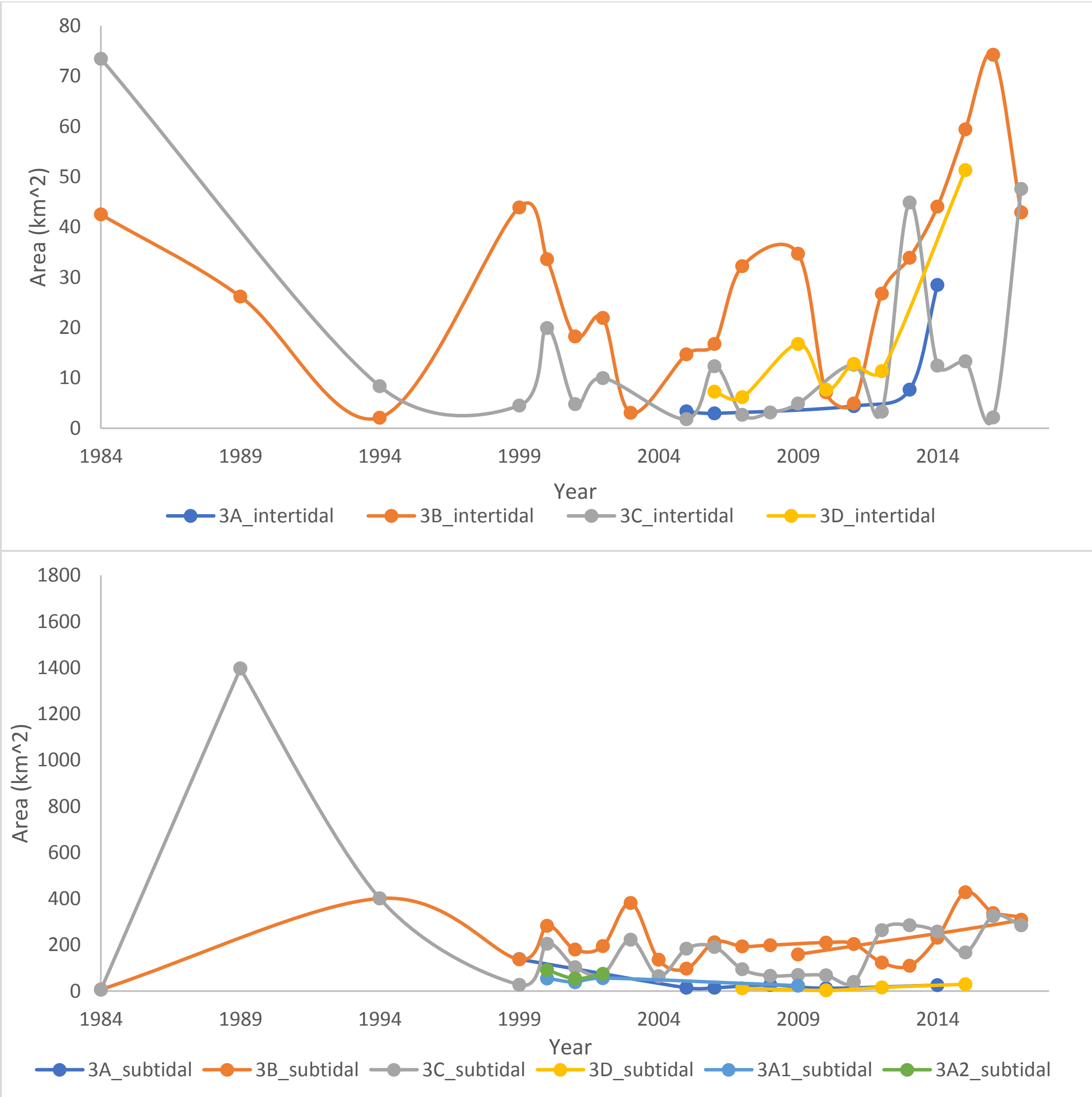

Figure 14. Changes in area of the intertidal (upper graph) and subtidal (lower graph) banks in section 3 from 1984 till 2017.

4.2.4 Berbice River - Courantyne River (Figures 15 and 16)

This section starts with three mudbanks in 1984-1988, of which mudbank A slowly seems to become land from 1984 till 1998. In 1999 only B and C are left and they have moved north westward compared to 1984. From 2003 more sediment starts to accumulate on the left side of the Courantyne River and in 2005 a new bank is visible. The banks start to grow and sometimes they even seem to merge. From 2011 till 2017 a large part of the left bank of the delta is covered with mudbank.

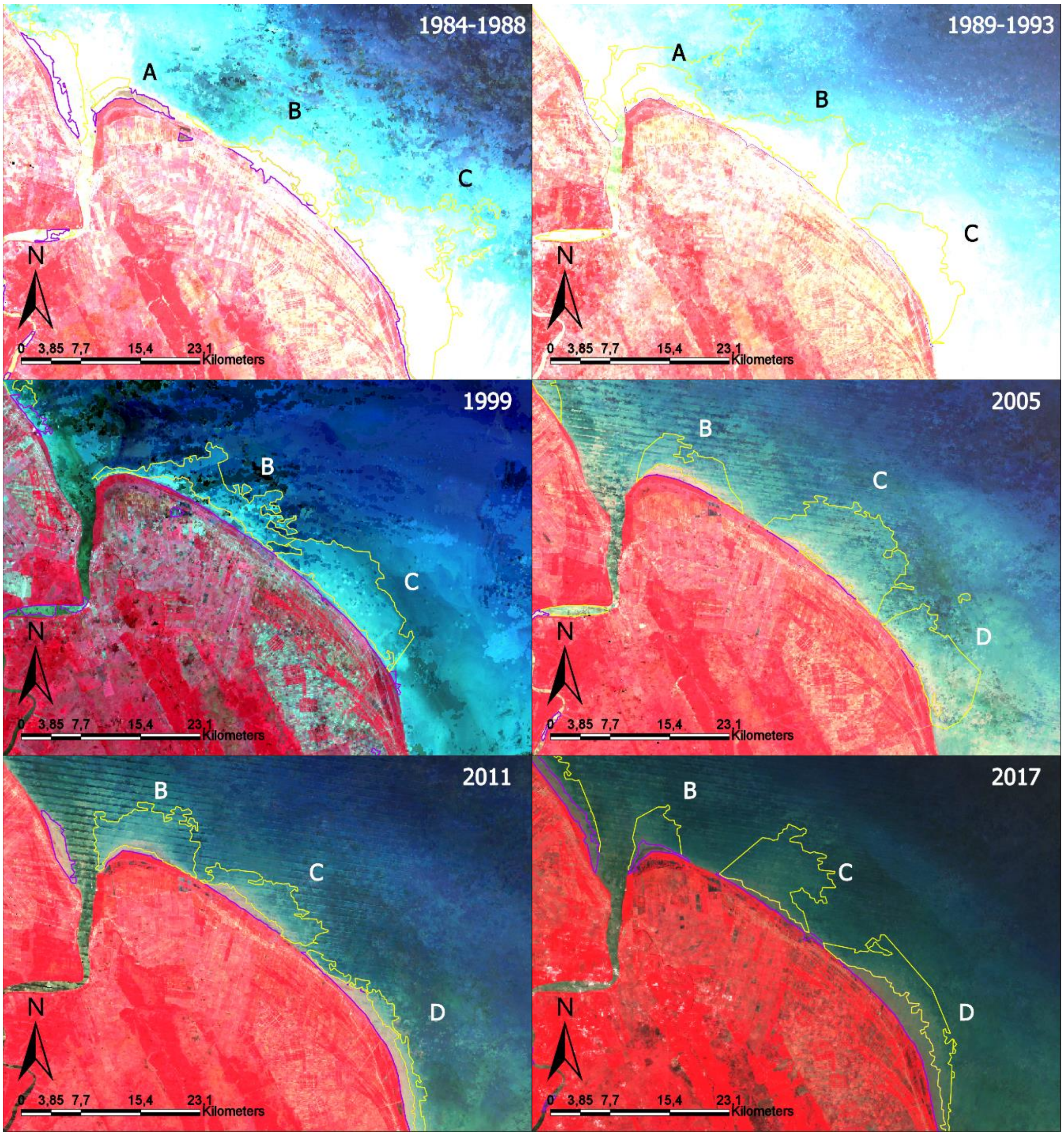

Figure 15. The mudbanks from Section 4 in a selection of the research period.

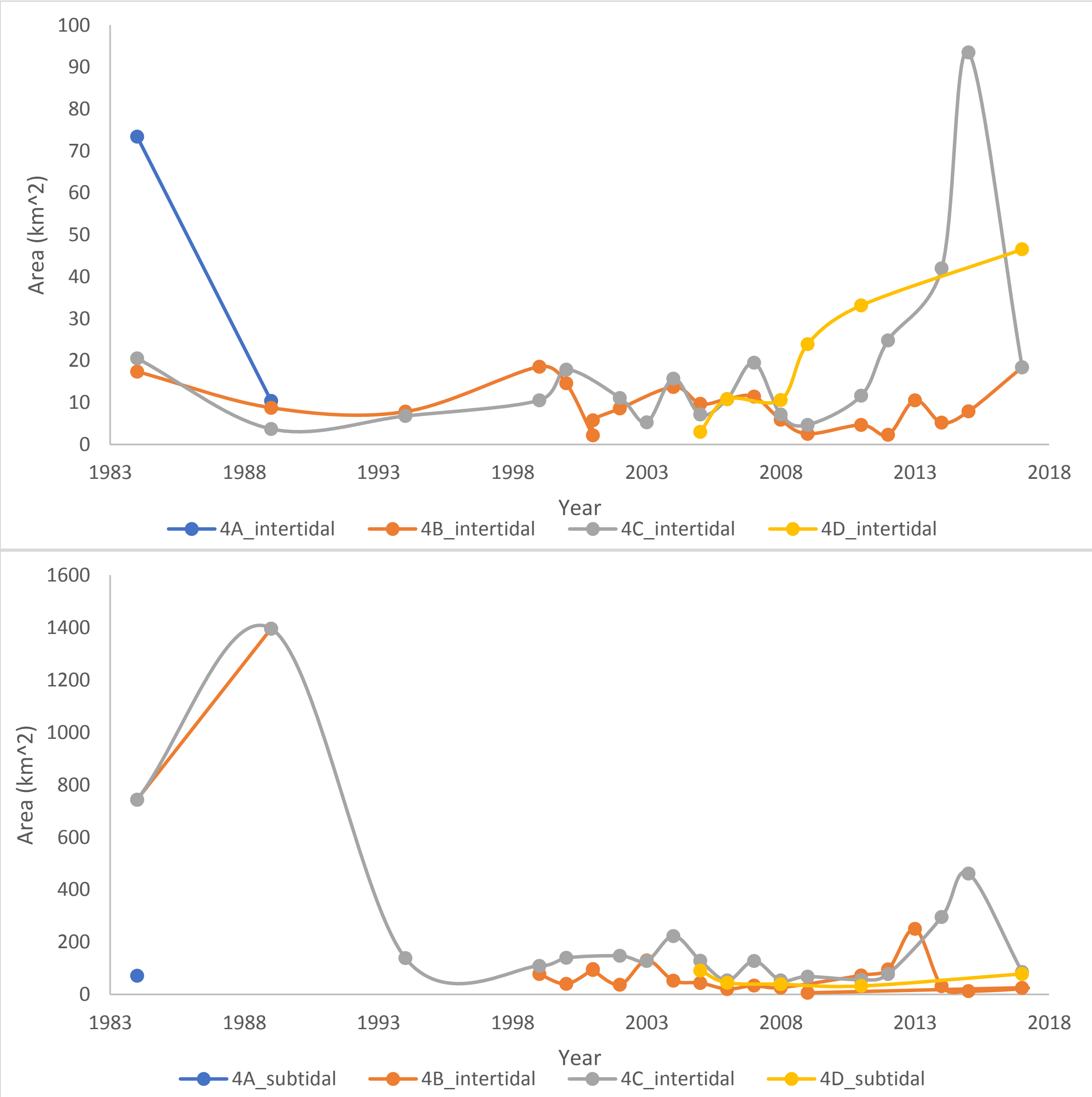

Figure 16. Changes in area of the intertidal (upper graph) and subtidal (lower graph) banks in section 4 from 1984 till 2017.

4.2.5 Courantyne River – Coppename River (Figures 17 and 18)

In 1984-1988 there are three mudbanks in this area, of which C is the smallest. In 1989-1993 the banks have grown and moved to the north west. In 1994-1998 bank C has almost disappeared, but in 1999 it has grown again and is clearly visible. The banks keep moving and in 2001 bank A splits into two. Bank C grows larger and its beginning moves more into the Coppename River. In 2006 the banks suddenly become smaller, bank A1 almost disappears. In 2007 Bank C splits into C1 and C2.

In 2011 bank A1 disappears and C2 becomes very small. C2 grows a little but then disappears in 2015, leaving only A2, B and C1 till 2017.

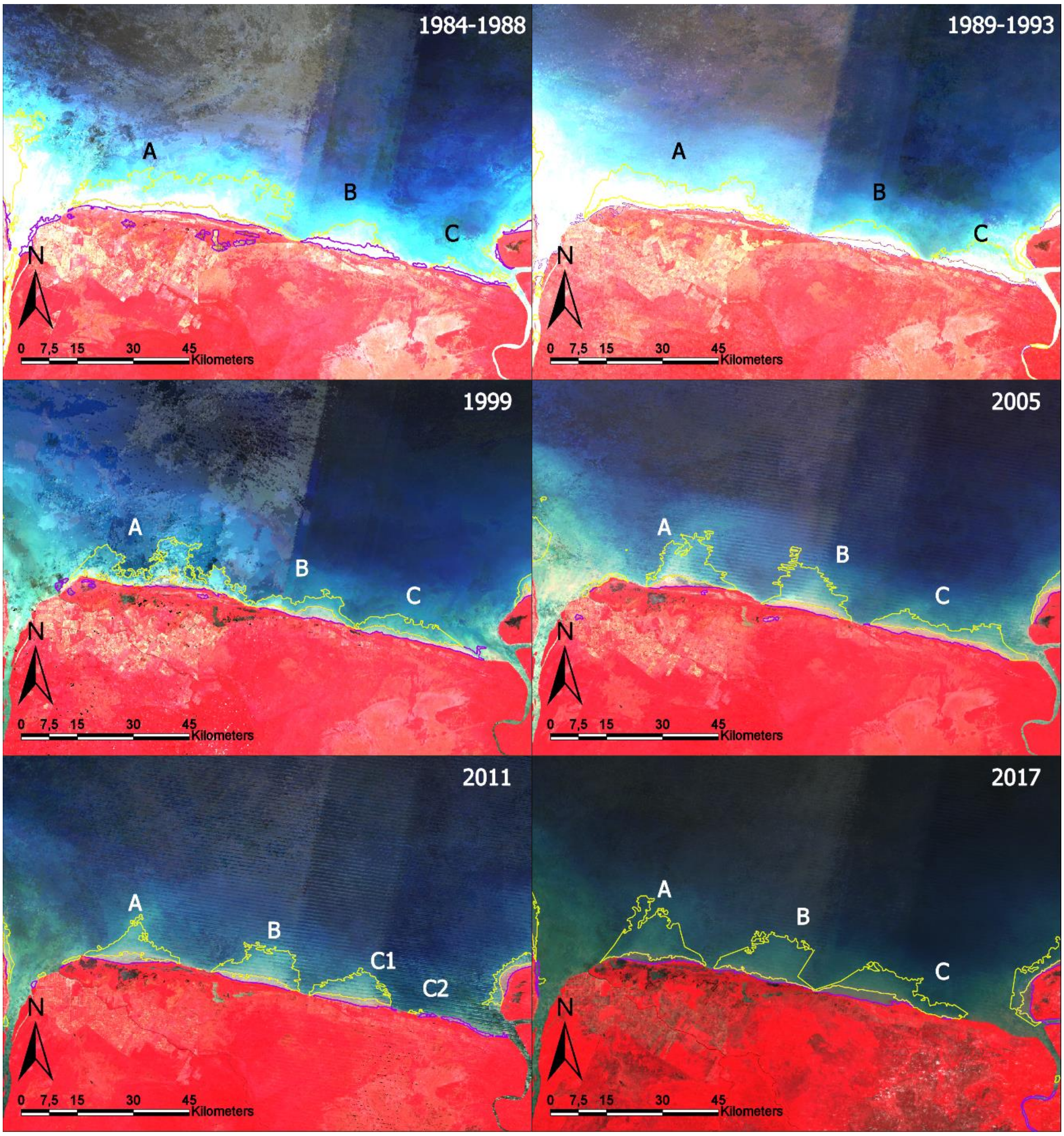

Figure 17. The mudbanks from Section 5 in a selection of the research period.

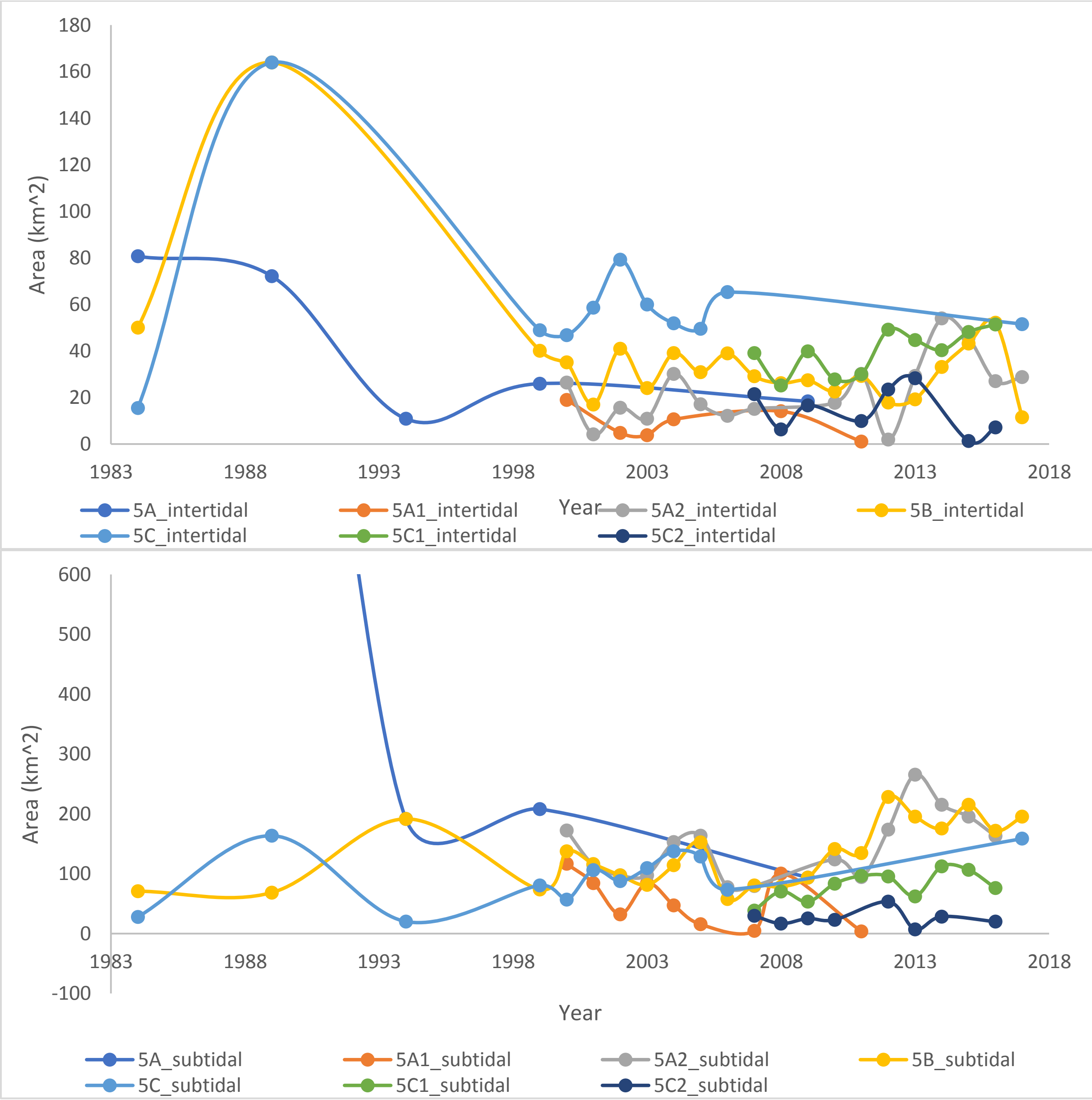

Figure 18. Changes in area of the intertidal (upper graph) and subtidal (lower graph) banks in section 4 from 1984 till 2017.

4.2.6 Coppename River – Suriname River (Figures 19 and 20)

From 1984 till 1993 the complete coast between these rivers is covered with one mudbank that has a long elongated intertidal part and a large subtidal plume. In 1994-1998 the subtidal plume has become less clear and it the bank is less elongated but starts to form two separate bulges. In 2000 a third bulge starts to appear and this bank with three bulges remains till in 2007 it splits into two banks. These banks start to grow and the right one, A2 quickly becomes larger. As the banks move to the left they merge again in 2010 and one long bank with a large plume arises again, very similar to the one from 1984 till 1993.

Apart from this big bank there is also a smaller bank that sometimes appears left to bank A. This bank sporadically appears and disappears, but from 2010 the bank A moves closer to this area and it becomes a more permanent bank as part of bank A.

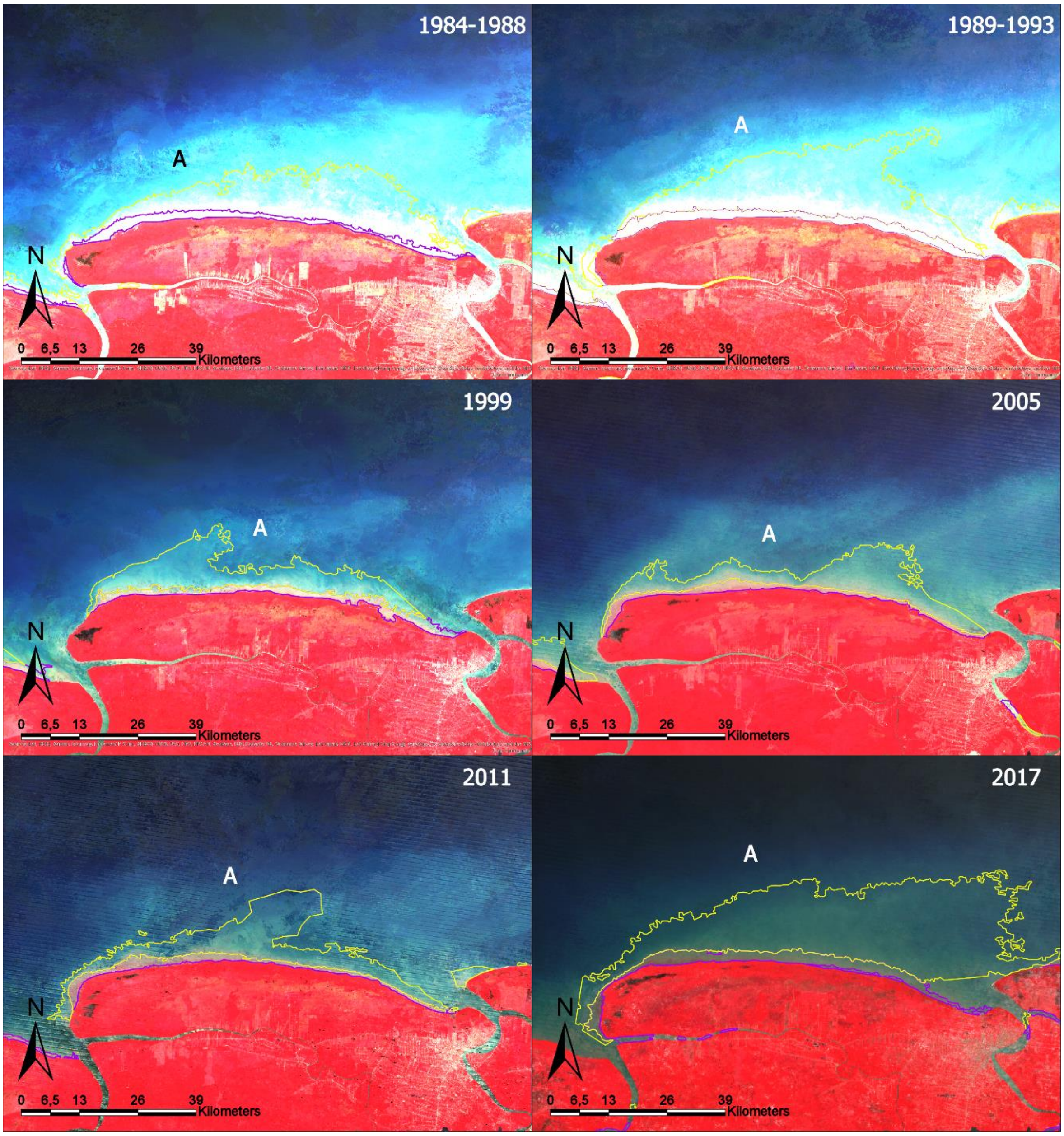

Figure 19. The mudbanks from Section 6 in a selection of the research period.

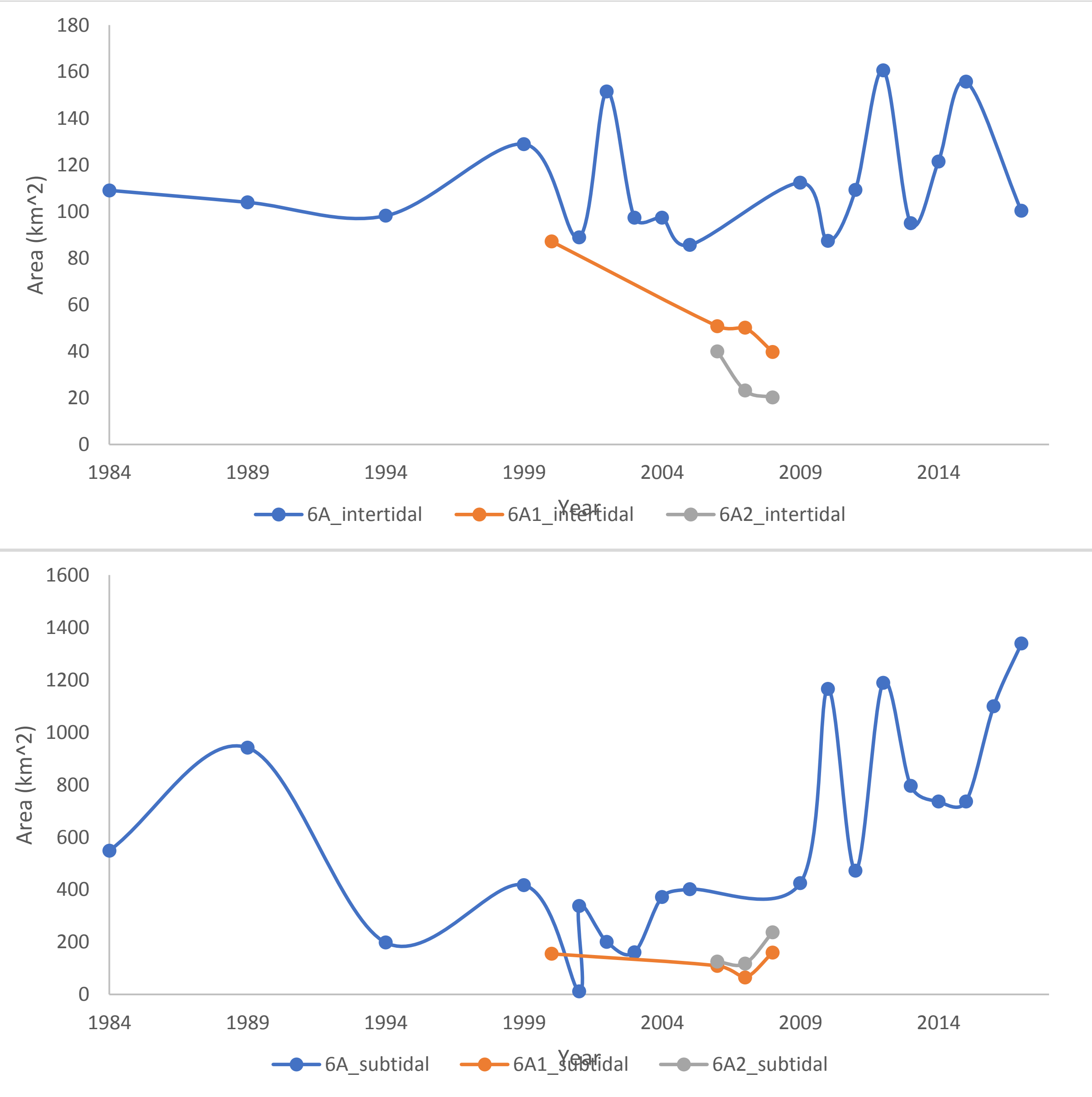

Figure 20. Changes in area of the intertidal (upper graph) and subtidal (lower graph) banks in section 6 from 1984 till 2017.

4.2.7 Suriname River – Maroni River (Figures 21 and 22)

This section there is one long bank (B) with a large plume that remains there from 1984 till 1998. In 1999 the plume becomes smaller, but from 2003 it gradually starts to grow again as it moves to the left. Also, a smaller bank (bank A) appears left of bank B. This bank disappears in 2005, 2008 and from 2012 till 2014. In 2015 it appears again and slowly merges with bank B.

In 2003 a third bank has emerged on the right (C), near the Maroni River. From 2007 on the bank steadily grows, apart from the years 2010 and 2014 in which the banks suddenly become smaller. This banks also moves to the left, in a northwestern direction.

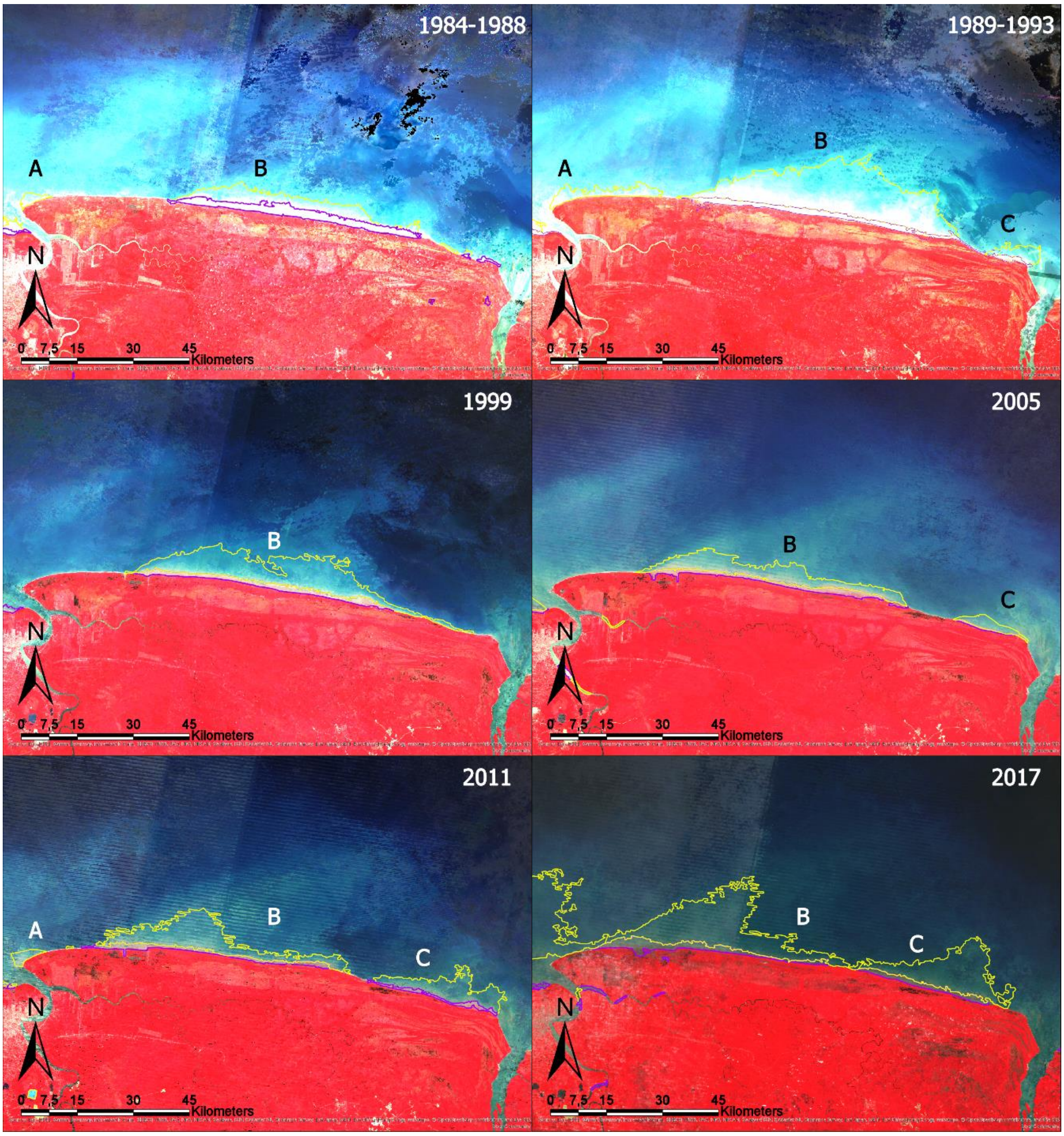

Figure 21. The mudbanks from Section 7 in a selection of the research period.

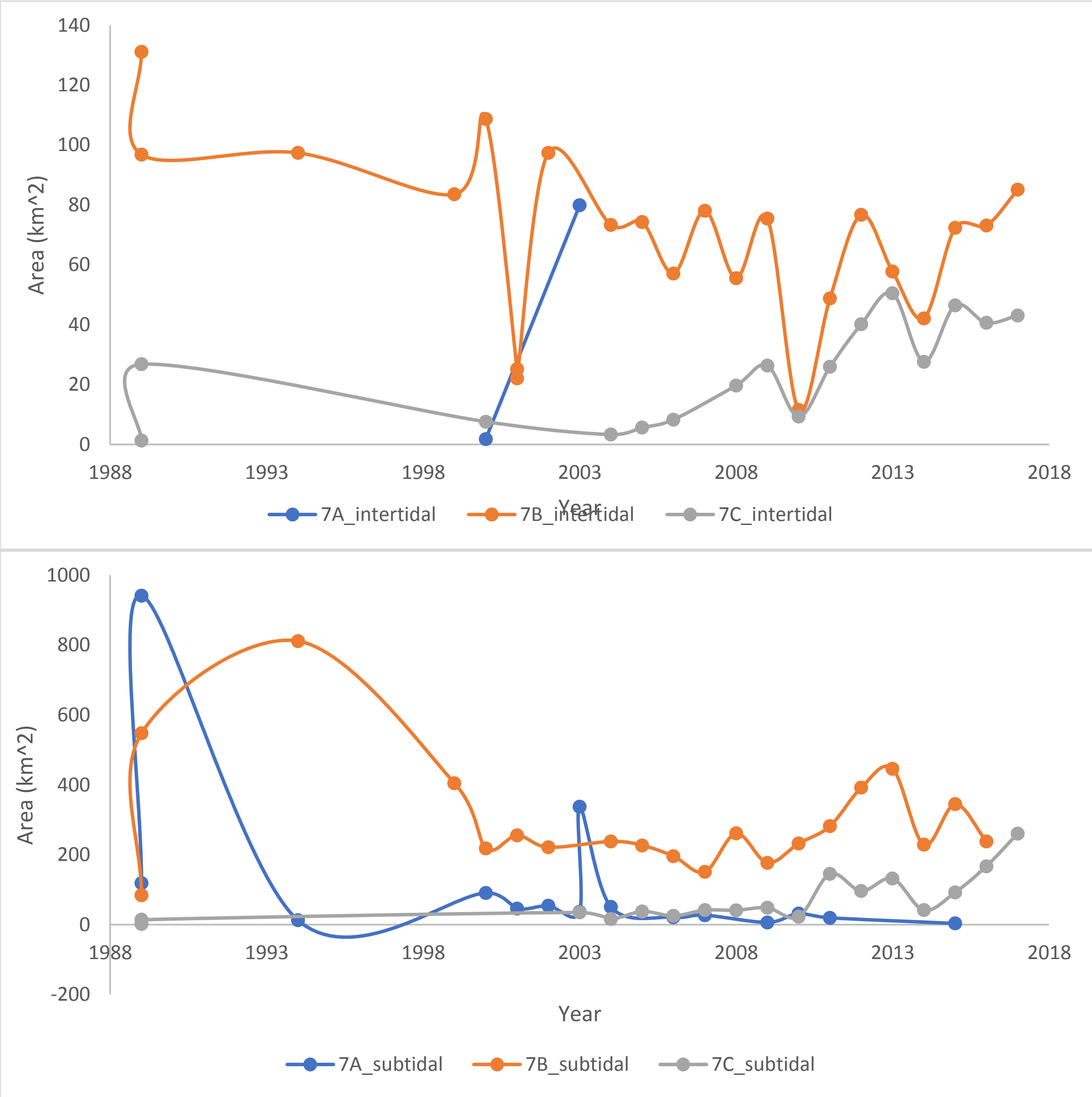

Figure 22. Changes in area of the intertidal (upper graph) and subtidal (lower graph) banks in section 7 from 1988 till 2017.

4.2.8 Maroni River -Sinnamary River (Figures 23 and 24)

For the period 1984 till 1998 only the section from the Maroni river till the Counamama River is covered. During this period there are three mudbanks in this section. In 1984-1988 bank C is mostly visible on the right side of the Counamama River. In 1989-1993 this section is not completely visible but in 1994-1998 this bank has moved more to the left and is largely on the left side of the river.

The other banks also clearly move to the left. In 1994-1998 Bank A is at the mouth of the Maroni River and the piece of land near Mana that it just passed has become thinner.

From the data from 1999 it becomes clear that there is a fourth mudbank (D) lying over the mouth of the Sinnamary River. This is the largest bank of this section.

On the left side of the section at bank A the land bridge near Mana has disappeared and a small island is now in the center of the mudbank. Bank A decreases in size until in 2004 only a small stroke of mudbank remains on the south side of the little island. It stays like this till bank B has move enough to the left to cross the Mana River mouth in 2010. Now the small island becomes attached to the mainland and the bank remains on both side until it passes the river mouth and becomes smaller again in 2017.

Bank C and D vary little in size as they slowly move to the left. Bank D is split up from 2001 as it moves over the Sinnamary River, but it merges again in 2013 as the entire bank has past the mouth. When in 2017 Bank D is moving over the Counamama River it seems as if it merges with Bank C.

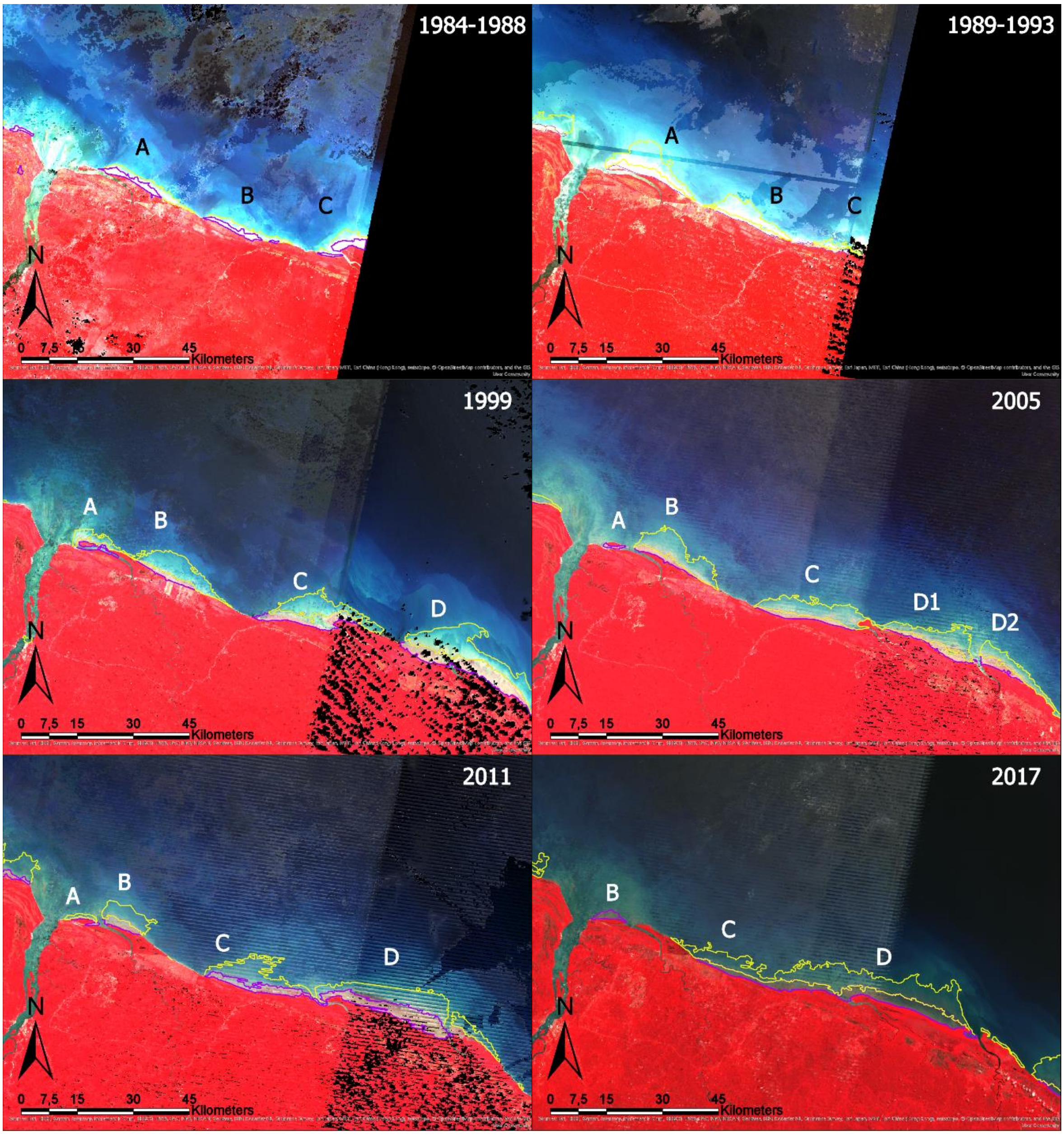

Figure 23. The mudbanks from Section 8 in a selection of the research period. The letters are placed at the right mudbanks for identification.

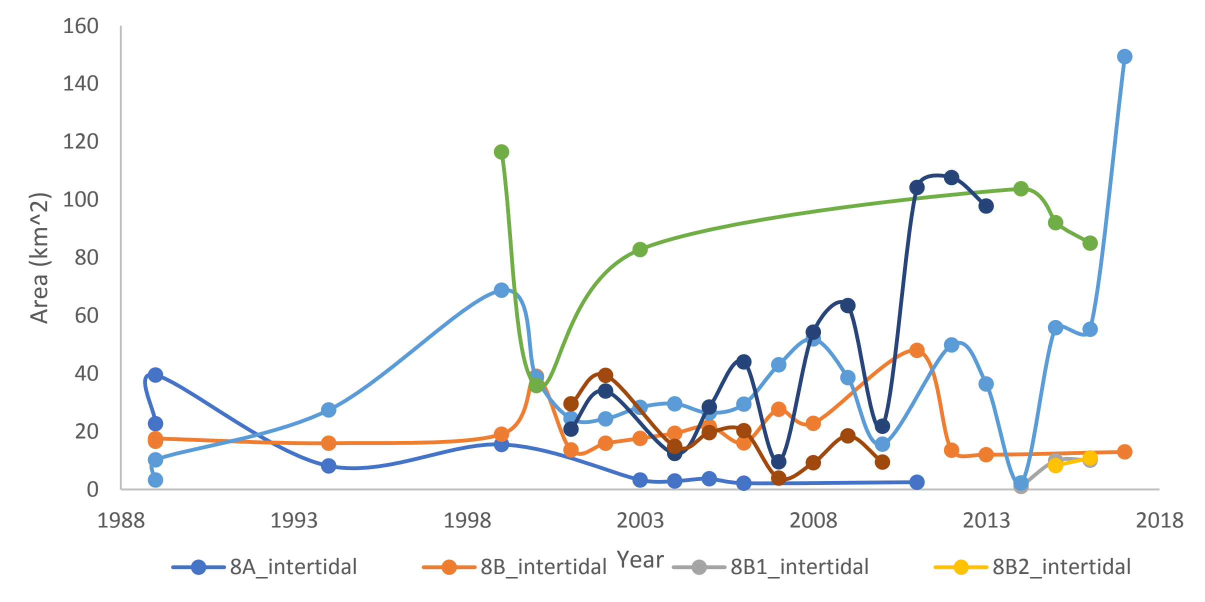

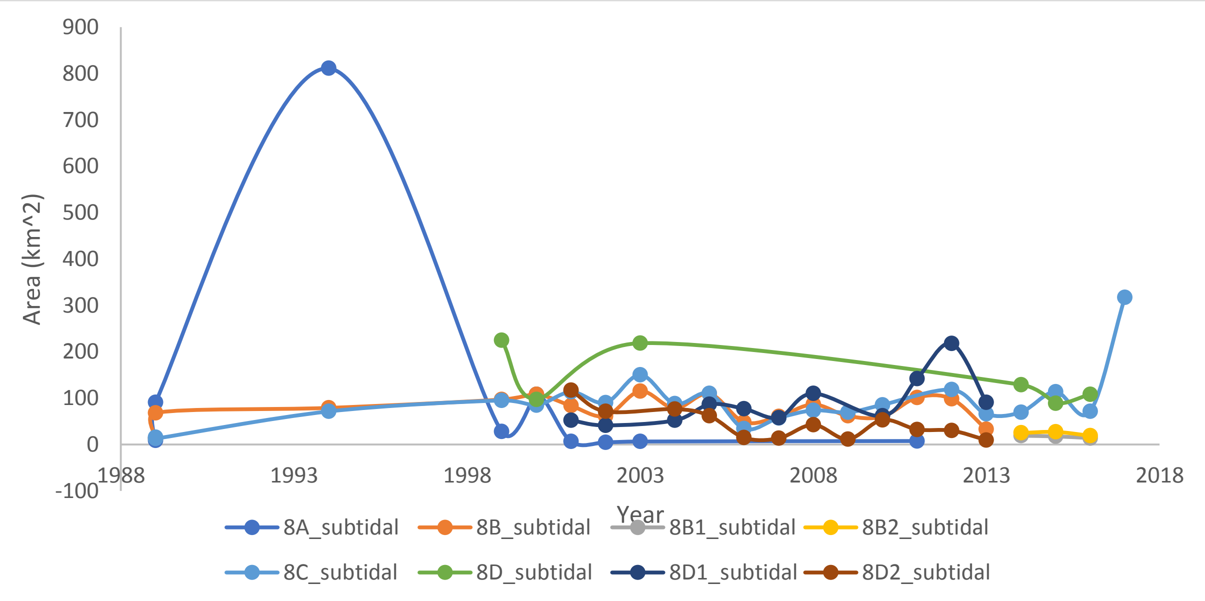

Figure 24. Changes in area of the intertidal (upper graph) and subtidal (lower graph) banks in section 8 from 1988 till 2017.

4.2.9 Sinnamary River - Approuague River (Figures 25 and 26)

This section starts with three large mudbanks in 1999. They become a bit smaller after 2000 and in 2004 bank C has become more elongated.

In 2002 another small bank emerges between the Cayenne River and the Mahury River. This bank moves to the left side of this small peninsula and disappears in 2008. In this year Bank B and C merge into one larger bank. In 2009 a new bank (D) emerges just south of Bank A. At the Cayenne River mouth a new bank (E) seems to form as well. In 2010 bank A splits in two as it passes the Kourou River. Bank E is now clearly visible. In 2010 Bank B and C have become separate banks again as they passed over the Kaw River.

In 2011 Bank A merges again and Bank D and E also merge. The banks continue to move northwestward. Bank B and C sometimes form a whole and sometimes are separate. However, in

2016 Bank B and C become more fragmented and in 2017 the left part (bank B) is clearly larger than bank C.

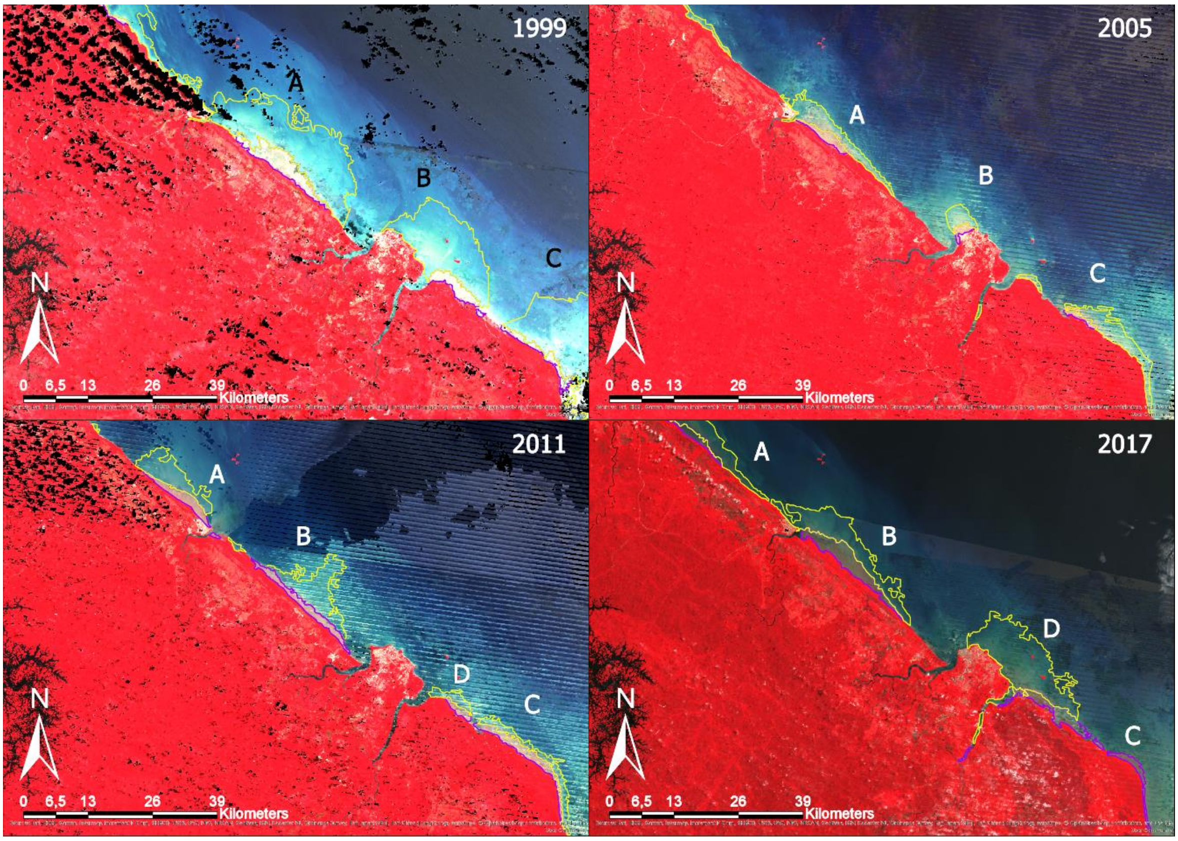

Figure 25. The mudbanks from Section 9 in a selection of the research period.

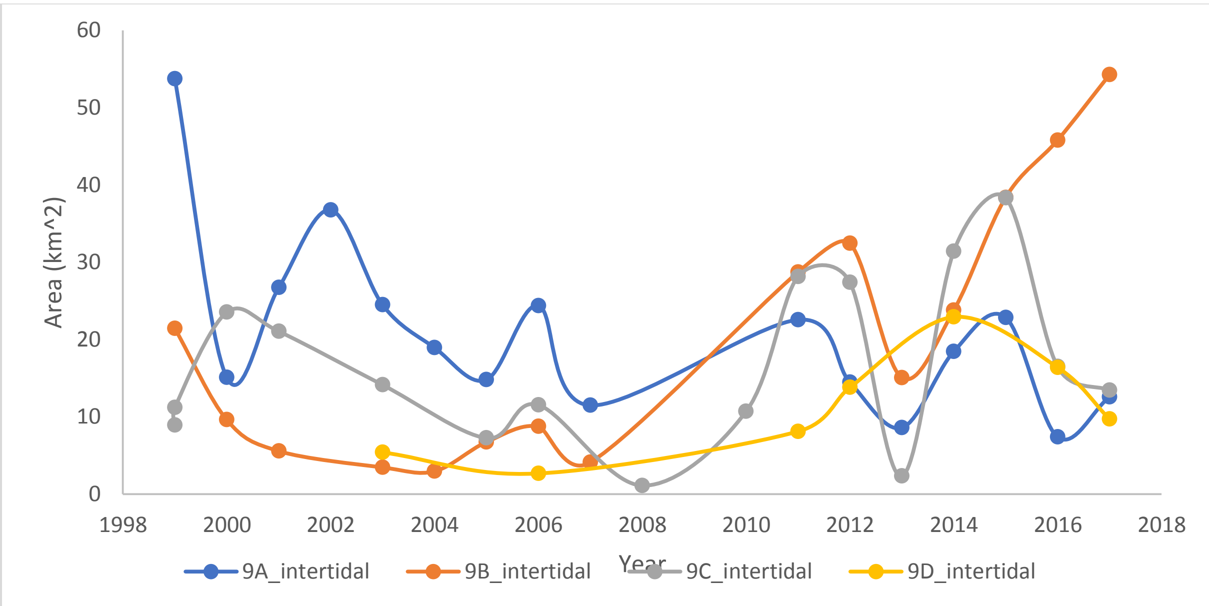

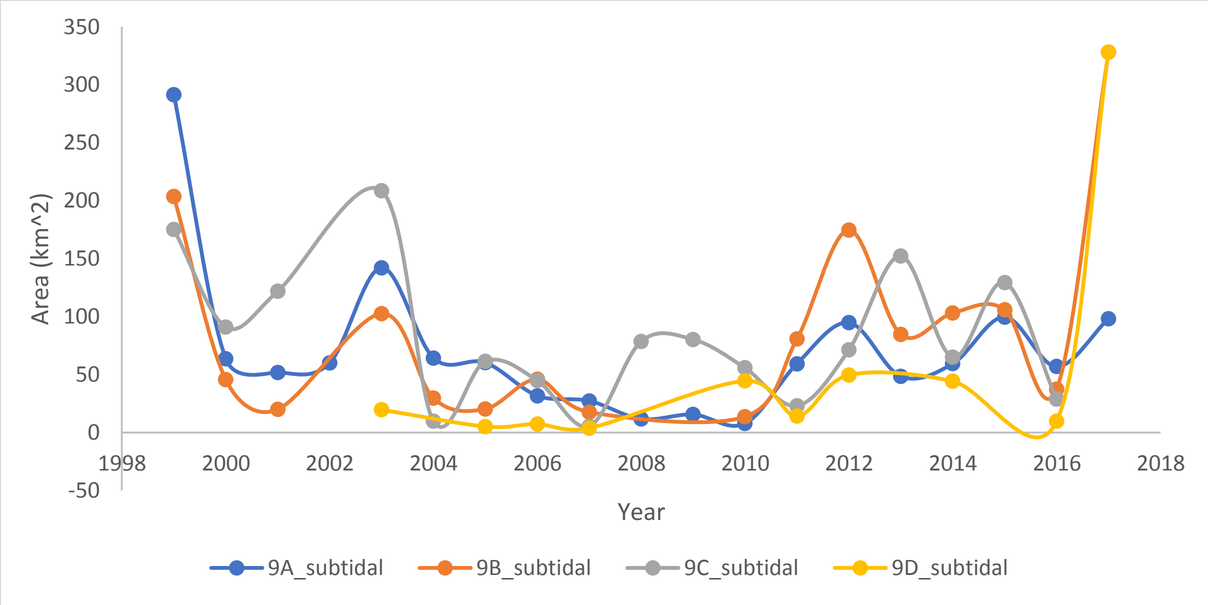

Figure 26. Changes in area of the intertidal (upper graph) and subtidal (lower graph) banks in section 9 from 1999 till 2017.

5. Discussion

This research looked at the spatial distribution of mudbanks along the Guiana coastline between 1984 and 2017. During this period the dominant migration was in a northwest direction causing the banks to move from the Amazon river towards the Orinoco river. Along this track the mudbanks changed in terms of form and size and the number of mudbanks changed because of splitting and merging of banks. Additionally, the coast changed as well, accumulating in some areas and eroding in others, which is interesting to know for making strategies to protect coastal areas from flooding and erosion.

5.1 Accuracy assessment

Before discussing any of the results it is necessary to mention the different possible errors in the methods used that could have resulted in wrong interpretations of the mudbanks. First the CART classification that was used shows an accuracy of 83 -87 % (Goldblatt et al. 2016). This means that nearly 20% of the changes seen in the different banks are the result of classification errors. To minimalize the errors the classifications were compared to the original satellite images and some of the wrong classifications were adjusted. To get an even better accuracy assessment the final mudbank images, after the clean-up in ArcGIS Pro, should be used in the assessment and compared to training data from the satellite images.

Besides the errors in the classification there are also some gaps in the classifications due to the lack of Landsat images in the period of 1984 till 1999. This means that some of the trends that are found do not necessarily apply for this period.

5.2 Form, size and number of mudbanks

Along the entire coast mudbanks are moving in a northwestward direction during which they change in size and form. Most of the mudbanks have an elongated intertidal area that runs along the coastline (Figure 19). The subtidal part is often either a rounded form (Figure 23) or a more triangle like a plume (Figure 19) Most times the plume deflects in a southeast direction, but in the area east of the Sinnamary River (Section 8 and 9) the plume deflects in the other direction (Figure 25).

When mudbanks arrived at a river mouth they often became smaller as they passed over it. The bank often splits up, but merges again when it has passed the river, for example bank 8D in section 8. However, when passing a larger river, for example the Maroni River in Section 8, the bank would become smaller and finally disappear. Although, at approximately the same time that the mudbank disappeared on the right side of the Marino River in Section 8 a new bank also started to form on the left side of the river in section 7. It is very likely that this is the same bank because according to Anthony, Gardel and Gratiot (2014) river mouth jets do not lead to disintegration or liquefaction of mudbanks. This is partially because of the size of the banks and because the rivers have a lower discharge for a part of the year (Anthony et al. 2014).

Mudbanks do not only split or merge when they pass a river. In Section 6 a large mudbank breaks up into three smaller banks even when there are no river mouths in this area. The splitting of the mudbanks is the result of erosion, which can have several causes. Seafront erosion of the mudbank due to wave action occurs when there is not enough soft mud in front of the mudbank which is the result of alongshore mud migration (Gensac et al. 2015). Due to climate change the water levels are rising in the area with a lowest projection of 2 mm per year. This rise in water level contributes to the erosive power of nearshore currents and waves, causing more erosion to the coastline (Ahmad and Lakhan 2012). Another a result of climate change is an increase in tropical and North Atlantic storms that generate waves, causing erosion to the coast (Anthony and Gratiot 2012). In section 4, the two mudbanks clearly become smaller in 2005 and they are split up into three banks. This falls together with the extreme wave event of October 2005, which caused massive flooding and erosion in this area. The extreme wave heights were the result of a severe depression in the Northern Atlantic Ocean during October 11 -15 (van Ledden et al. 2009).

Since the early 2000s an increase in mud bars is seen along the coast. These bars are often short-lived features in front of the mudbanks that are reworked and pushed shoreward by waves. The observed increase of mud bars is also the result of increased wave forcing that cause the mobilization of offshore fluid mud deposits (Gardel et al. 2011). Although increased wind and wave action can cause more erosion to the coastline and mudbanks, depending on their direction it can also result in a redistribution of mud (Anthony et al. 2014; Wanless and Tagett 1989). This a logical explanation for why one bank is reduced in size while the next bank is growing. Mud eroded from one bank is reworked and transported to the following bank.

The natural causes for erosion are amplified in areas were humans disturb the mudbank interactions along the coast. For example, mangrove forests along the coast of Surinam and Guyana are significantly reduced for agricultural or aquaculture purposes. The erosion of mangroves can strongly reduce the efficiency of mudbanks in dissipating wave energy, which again can lead to more erosion (Anthony and Gratiot 2012).

5.3 Forming of new mudbanks

Most of the new mudbanks that were formed are the result of the splitting of larger mudbanks. A completely new mudbank were expected to form in Section 9, near Cabo Cassipore. There were many changes in the mudbanks in this area, but there was not a clear forming of a separate new mudbank.

On the left side of some of the larger rivers, like the Essequibo and the Marino Rivers, some mudbanks do seem to have formed. First some sediment accumulates till it becomes a larger bank and it moves slowly out of the river mouth. It is possible that these mudbanks are not new mudbanks, but banks that moved from one side of the river to the other side. It seems as if these mudbanks have disappeared, but it is very well possible that the sediment needs some time to accumulate on the other side of these rivers, as they have a stronger current than the smaller rivers. The timing often seems right. For both the Essequibo River as the Marino River a mudbank disappeared into the river mouth in the period before the emerging of the new mudbank.

More research and extensive tracking of the sediments in these larger river mouth areas could give confirmation on if these are the same banks before and after the river mouth. Perhaps sampling of the muds in the banks before and after the mouth could show if they originated from the same bank.

5.4 Accumulation and erosion along the coast

Areas with mudbanks in front of them are associated with accumulation. A clear example of this can be found in Section 4. In the period 1984 -1998 a part of one of the mudbanks slowly has become part of the mainland. This shows that sometimes mudbanks protect the coast enough that sometimes part of the intertidal mudbank becomes part of the mainland.

Another example of accumulation and erosion is the area around Mana. Part of the land extended in a long thin stroke into the ocean. This area was protected by a mudbank. However, when the bank had moved away the arm eroded and only a small island remained. When there was a new mudbank in the area since 2013, it was protected again. Accumulation took place and now the island is attached to the mainland again.

Phases of accumulation and erosion in along the Guiana Coast between the eighteenth and twentieth centuries have been identified (Plaziat and Augustinus 2004). There are cyclical alternations of accretion and erosion phases visible along the Guianese coast, with a net accretion phase in 1951-1966 and erosion period in 1966-1991, followed by and accretion phase till at least 1999. These fluctuations are associated with the tides and wave action influenced by trade wind patterns (Augustinus 2004; Fromard, Vega, and Proisy 2004; Gratiot, Gardel, and Anthony 2007). In the period 1953 – 1986 there was an increase in the frequency and velocity of wind from an east-north east direction. In the period till 2004 there occurred a reverse of these trends, which results in an increase of longshore wave energy flux in coastal waters for coastal sections that are east-west directed, like the coast of Suriname. This should result in an increase in the length of the mudbanks (Augustinus 2004). In this period the results show elongated mudbanks along the Surinam coast, which fits with this theory.

6. Conclusion

The results from this thesis show that there are many factors influencing the mudbank dynamics along the Guiana Coastline. The number of mudbanks changes due to splitting and merging which is the result of the sediment distribution in the area. Due to erosion mudbanks can be split up. This erosion is caused by wave action which depends on the strength and direction of the trade winds but also on the occurrence of storms. Due to climate change the sea level will rise and tropical of North Atlantic storms are more likely to occur, both resulting in more erosion. Due to redistribution of the sediment, enhanced erosion in one area can result in more sediment apply to another area.

Apart from the natural processes of sediments distribution, humans also play a role in the mudbank dynamics. Man-made changes to the shoreline has amplified erosion in certain areas, causing the mudbanks to become smaller.

When looking at the formation of new mudbanks no clear example was found during this research period. This could be because the data of the section were the new bank would emerge is missing or because there simply has not formed a new bank. Along some river mouths new banks did seem to appear, but these could also be the result of an older bank passing the river mouth.

By calculating the average speed over the period 1999 till 2017, a migration speed of approximately 1.5 km per year was found.

Two clear locations have been identified where accumulation or erosion took place during the research period. One is in Section 4, where the mudbank becomes part of the mainland. The other is near Mana, where erosion takes place when a mudbank moves away, but accumulation takes place after a new mudbank covers the coast again.

This confirms the hypothesis that suggested that mudbanks protect the coast from for example wave energy. This makes it possible for accumulation to take place. When the mudbanks move away the coast becomes exposed and it is vulnerable for erosion.

The Guiana Coastline is put under more and more stress due to climate change and human actions. This thesis shows the changes along the coast for the past 34 years, which helps to identify where the coast is changing the most and what has caused these changes. By using this information, predictions of future changes can be made. These predictions are used for new strategies to protect the coast for more erosion, which will save the people and the mangrove forests that live in this area.

Acknowledgements

References

Ahmad, Sajid Rashid and V. Chris Lakhan. 2012. “GIS-Based Analysis and Modeling of Coastline Advance and Retreat Along the Coast of Guyana.” *Marine Geodesy*.

Allison, M. A., C. A. Nittrouer, and L. E. C. Faria. 1995. “Rates and Mechanisms of Shoreface Progradation and Retreat Downdrift of the Amazon River Mouth.” *Marine Geology* 125(3–4):373–92. Retrieved May 2, 2018 (https://www.sciencedirect.com/science/article/pii/002532279500020Y).

Allison, M. A., C. A. Nittrouer, and G. C. Kineke. 1995. “Seasonal Sediment Storage on Mudflats Adjacent to the Amazon River.” *Marine Geology*.

Allison, Mead A., Michael T. Lee, Andrea S. Ogston, and Robert C. Aller. 2000. “Origin of Amazon Mudbanks along the Northeastern Coast of South America.” *Marine Geology* 163(1–4):241–56. Retrieved April 30, 2018 (https://www.sciencedirect.com/science/article/pii/S0025322799001206).

Anthony, Edward J. et al. 2010. “The Amazon-Influenced Muddy Coast of South America: A Review of Mud-Bank–shoreline Interactions.” *Earth-Science Reviews* 103(3–4):99–121. Retrieved May 1, 2018 (https://www.sciencedirect.com/science/article/pii/S0012825210001200#f0015).

Anthony, Edward J., Antoine Gardel, and Nicolas Gratiot. 2014. “Fluvial Sediment Supply, Mud Banks, Cheniers and the Morphodynamics of the Coast of South America between the Amazon and Orinoco River Mouths.” *Geological Society, London, Special Publications* 388(1):533–60. Retrieved May 1, 2018 (http://sp.lyellcollection.org/lookup/doi/10.1144/SP388.8).

Anthony, Edward J. and Nicolas Gratiot. 2012. “Coastal Engineering and Large-Scale Mangrove Destruction in Guyana, South America: Averting an Environmental Catastrophe in the Making.” *Ecological Engineering* 47:268–73. Retrieved July 8, 2018 (https://www-sciencedirect-com.proxy.library.uu.nl/science/article/pii/S092585741200256X).

Augustinus, P. G. E. F. 1978. “The Changing Shoreline of Suriname (South America).” Retrieved May 18, 2018 (https://www.narcis.nl/publication/RecordID/oai:dspace.library.uu.nl:1874%2F263140).

Augustinus, Pieter G. E. .. 2004. “The Influence of the Trade Winds on the Coastal Development of the Guianas at Various Scale Levels: A Synthesis.” *Marine Geology* 208(2–4):145–51. Retrieved July 8, 2018 (https://www-sciencedirect-com.proxy.library.uu.nl/science/article/pii/S0025322704001045).

Breiman, Leo. 1984. *Classification and Regression Trees*. Chapman & Hall. Retrieved July 7, 2018 (https://books.google.nl/books?id=JwQx-WOmSyQC&redir_esc=y).

Bulgakov, N. P., S. N. Bulgakov, and V. N. Eremeev. 1998. “Guiana Current over North Brazil Shelf and Continental Slope.” *Physical Oceanography* 9(1):55–70. Retrieved May 17, 2018 (http://link.springer.com/10.1007/BF02523027).

Chander, Gyanesh, Brian L. Markham, and Dennis L. Helder. 2009. “Summary of Current Radiometric Calibration Coefficients for Landsat MSS, TM, ETM+, and EO-1 ALI Sensors.” *Remote Sensing of Environment* 113(5):893–903. Retrieved July 5, 2018 (https://www.sciencedirect.com/science/article/pii/S0034425709000169#!).

Eisma, D., P. G. E. F. Augustinus, and C. Alexander. 1991. “Recent and Subrecent Changes in the Dispersal of Amazon Mud.” *Netherlands Journal of Sea Research* 28(3):181–92. Retrieved April 30, 2018 (https://www.sciencedirect.com/science/article/pii/007775799190016T).

Farda, N. M. 2017. “Multi-Temporal Land Use Mapping of Coastal Wetlands Area Using Machine Learning in Google Earth Engine.” *IOP Conference Series: Earth and Environmental Science* 98(1):012042. Retrieved July 6, 2018 (http://stacks.iop.org/1755-1315/98/i=1/a=012042?key=crossref.a06cbb12b837c952ec652716788655fd).

Foga, Steve et al. 2017. “Cloud Detection Algorithm Comparison and Validation for Operational Landsat Data Products.” *Remote Sensing of Environment* 194:379–90. Retrieved July 6, 2018 (https://www.sciencedirect.com/science/article/pii/S0034425717301293?via%3Dihub).

Froidefond, J. .., M. Pujos, and X. Andre. 1988. “Migration of Mud Banks and Changing Coastline in French Guiana.” *Marine Geology* 84(1–2):19–30. Retrieved April 30, 2018 (https://www.sciencedirect.com/science/article/pii/0025322788901223).

Fromard, F., C. Vega, and C. Proisy. 2004. “Half a Century of Dynamic Coastal Change Affecting Mangrove Shorelines of French Guiana. A Case Study Based on Remote Sensing Data Analyses and Field Surveys.” *Marine Geology* 208(2–4):265–80. Retrieved July 8, 2018 (https://www-sciencedirect-com.proxy.library.uu.nl/science/article/pii/S0025322704001112#FIG3).

Gardel, A., E. Gensac, … EJ Anthony-…. 2011–Proceedings of, and Undefined 2011. 2011. “Wave-Formed Mud Bars: Their Morphodynamics and Role in Opportunistic Mangrove Colonization.” *Journal of Coastal Research, Special* No. 64:384–87. Retrieved July 8, 2018 (https://www.researchgate.net/profile/Hubert_Loisel/publication/235003844_Wave-formed_mud_bars_Their_morphodynamics_and_role_in_opportunistic_mangrove_colonization/links/0fcfd5103b0c498c0b000000.pdf).

Gensac, Erwan, Antoine Gardel, Sandric Lesourd, and Laurent Brutier. 2015. “Morphodynamic Evolution of an Intertidal Mudflat under the Influence of Amazon Sediment Supply – Kourou Mud Bank, French Guiana, South America.” *Estuarine, Coastal and Shelf Science* 158:53–62. Retrieved June 25, 2018 (https://www-sciencedirect-com.proxy.library.uu.nl/science/article/pii/S0272771415000864#sec5).

Goldblatt, Ran, Wei You, Gordon Hanson, and Amit Khandelwal. 2016. “Detecting the Boundaries of Urban Areas in India: A Dataset for Pixel-Based Image Classification in Google Earth Engine.” *Remote Sensing* 8(8):634. Retrieved July 4, 2018 (http://www.mdpi.com/2072-4292/8/8/634).

Gratiot, Nicolas, Antoine Gardel, and Edward J. Anthony. 2007. “Trade-Wind Waves and Mud Dynamics on the French Guiana Coast, South America: Input from ERA-40 Wave Data and Field Investigations.” *Marine Geology* 236(1–2):15–26. Retrieved July 8, 2018 (https://www-sciencedirect-com.proxy.library.uu.nl/science/article/pii/S0025322706002295).

Kineke, G. C., R. W. Sternberg, J. H. Trowbridge, and W. R. Geyer. 1996. “Fluid-Mud Processes on the Amazon Continental Shelf.” *Continental Shelf Research* 16(5–6):667–96. Retrieved April 30, 2018 (https://www.sciencedirect.com/science/article/pii/027843439500050X).

van Ledden, Mathijs, Geoffrey Vaughn, Joost Lansen, Frank Wiersma, and Mewburn Amsterdam. 2009. “Extreme Wave Event along the Guyana Coastline in October 2005.” *Continental Shelf Research* 29(1):352–61. Retrieved July 10, 2018 (https://www.sciencedirect.com/science/article/pii/S0278434308001118).

Mertens, Marion, Inga Nestler, and Bernd Huwe. 2002. “GIS-Based Regionalization of Soil Profiles with Classification and Regression Trees (CART).” *Journal of Plant Nutrition and Soil Science* 165(1):39. Retrieved July 7, 2018 (http://doi.wiley.com/10.1002/1522-2624%28200202%29165%3A1%3C39%3A%3AAID-JPLN39%3E3.0.CO%3B2-X).

Metcalf, W. G. and M. C. Stalcup. 1967. “Origin of the Atlantic Equatorial Undercurrent.” *Journal of Geophysical Research* 72(20):4959–75. Retrieved May 17, 2018 (http://doi.wiley.com/10.1029/JZ072i020p04959).

Patel, Nirav N. et al. 2015. “Multitemporal Settlement and Population Mapping from Landsat Using Google Earth Engine.” *International Journal of Applied Earth Observation and Geoinformation* 35:199–208. Retrieved July 4, 2018 (https://www.sciencedirect.com/science/article/pii/S0303243414001998).

Pekel, Jean-François, Andrew Cottam, Noel Gorelick, and Alan S. Belward. 2016. “High-Resolution Mapping of Global Surface Water and Its Long-Term Changes.” *Nature* 540(7633):418–22. Retrieved July 6, 2018 (http://www.nature.com/articles/nature20584).

Plaziat, Jean-Claude and Pieter G. E. .. Augustinus. 2004. “Evolution of Progradation/Erosion along the French Guiana Mangrove Coast: A Comparison of Mapped Shorelines since the 18th Century with Holocene Data.” *Marine Geology* 208(2–4):127–43. Retrieved May 2, 2018 (https://www.sciencedirect.com/science/article/pii/S0025322704001033).

Rockwell Geyer, W. et al. 1996. “Physical Oceanography of the Amazon Shelf.” *Continental Shelf Research* 16(5–6):575–616. Retrieved May 18, 2018 (https://www.sciencedirect.com/science/article/pii/0278434395000518).

The Interior Department of USGS. 2018a. “PRODUCT GUIDE LANDSAT 4-7 SURFACE REFLECTANCE (LEDAPS) PRODUCT.” Retrieved July 7, 2018 (https://landsat.usgs.gov/sites/default/files/documents/ledaps_product_guide.pdf).

The Interior Department of USGS. 2018b. “PRODUCT GUIDE LANDSAT 8 SURFACE REFLECTANCE CODE (LASRC) PRODUCT.” Retrieved July 7, 2018 (https://landsat.usgs.gov/sites/default/files/documents/lasrc_product_guide.pdf).

USGS. 2017a. “USGS Landsat 4 Surface Reflectance Tier 1.” Retrieved July 7, 2018 (https://code.earthengine.google.com/dataset/LANDSAT/LT04/C01/T1_SR).

USGS. 2017b. “USGS Landsat 5 Surface Reflectance Tier 1.” Retrieved July 7, 2018 (https://code.earthengine.google.com/dataset/LANDSAT/LT05/C01/T1_SR).

USGS. 2017c. “USGS Landsat 7 Surface Reflectance Tier 1.” Retrieved July 7, 2018 (https://code.earthengine.google.com/dataset/LANDSAT/LE07/C01/T1_SR).

USGS. 2017d. “USGS Landsat 8 Surface Reflectance Tier 1.” Retrieved July 7, 2018 (https://code.earthengine.google.com/dataset/LANDSAT/LC08/C01/T1_SR).

USGS. 2018. “What Is the Worldwide Reference System (WRS)? | Landsat Missions.” Retrieved July 7, 2018 (https://landsat.usgs.gov/what-worldwide-reference-system-wrs).

Wanless, Harold R. and Matthew G. Tagett. 1989. “Origin, Growth and Evolution of Carbonate Mudbanks in Florida Bay.” *Bulletin of Marine Science,* 44(1):454–89. Retrieved July 8, 2018 (https://www-ingentaconnect-com.proxy.library.uu.nl/content/umrsmas/bullmar/1989/00000044/00000001/art00033#).

List of Figures

Considering that the figures in the results have the same captions with only the section numbers changing, they have been given here together:

List of Tables

Appendices

Appendix 1. Google Earth Engine script

```
var roi = /* color: #d63000 */ee.Geometry.Polygon(
      [[[-59.947153852172505, 9.537348901878355],
        [-60.2164829814983, 7.9661099200410845],
        [-59.23366164818253, 7.488307027263959],
        [-57.24493579253749, 5.8055468062264435],
        [-55.12822559368982, 5.584547017671924],
        [-53.11710188911002, 5.1762806909875465],
        [-52.22710472992901, 4.5182236832000235],
        [-52.218117610516856, 4.539059436675888],
        [-51.94599625535352, 5.573453582046353],
        [-51.96192415637006, 5.581414685957381],
        [-54.446920812752694, 6.7409954433034125],
        [-57.09639649569709, 7.013303176147607],
        [-59.815317914672505, 9.62942944844515]]]),
   L4 = ee.ImageCollection("LANDSAT/LT04/C01/T1_SR"),
   L5 = ee.ImageCollection("LANDSAT/LT05/C01/T1_SR"),
   L7 = ee.ImageCollection("LANDSAT/LE07/C01/T1_SR"),
   L8 = ee.ImageCollection("LANDSAT/LC08/C01/T1_SR"),

var yearStart = '2016'
var yearEnd = '2016'
var startD = [yearStart, '-01-01'].join('')
var endD = [yearEnd, '-12-31'].join('')
var maxSceneCloud = 80 //in percent

// Use this function to mask clouds in Landsat 8 imagery
var getBandsL8 = function(image) {
 var quality = image.select('pixel_qa');
 var cloud01 = quality.eq(61440);
 var cloud02 = quality.eq(53248);
 var cloud03 = quality.eq(28672);
 var mask = cloud01.or(cloud02).or(cloud03).not();
 return image.updateMask(mask);
};

// Remove clouds, add variables and filter to the area of interest
var cL8 = L8.filterBounds(roi)
                  .filterDate(startD, endD)
               .filterMetadata('CLOUD_COVER', 'less_than', maxSceneCloud) //by max cloudcover
                .map(getBandsL8) //add date, cloud, ndvi to the collection
                var newcL8 = cL8.select(['B3','B4','B5'], ['B2','B3','B4'])

// Use this function to mask clouds in Landsat 4, 5 and 7 imagery. (See
https://landsat.usgs.gov/collectionqualityband)
var getBandsL457 = function(image) {
 var quality = image.select('pixel_qa');
 var cloud01 = quality.eq(224);
 var cloud02 = quality.eq(160);
 var cloud03 = quality.eq(96);
 var mask = cloud01.or(cloud02).or(cloud03).not();
 return image.updateMask(mask);
};

// Remove clouds, add variables and filter to the area of interest
```

```
var cL4 = L4.filterBounds(roi)
        .filterDate(startD, endD)
        .filterMetadata('CLOUD_COVER', 'less_than', maxSceneCloud) //by max cloudcover
        .map(getBandsL457);

// Remove clouds, add variables and filter to the area of interest
var cL5 = L5.filterBounds(roi)
        .filterDate(startD, endD)
        .filterMetadata('CLOUD_COVER', 'less_than', maxSceneCloud) //by max cloudcover
        .map(getBandsL457) //add date, cloud, ndvi to the collection
// Remove clouds, add variables and filter to the area of interest
var cL7 = L7.filterBounds(roi)
          .filterDate(startD, endD)
        .filterMetadata('CLOUD_COVER', 'less_than', maxSceneCloud) //by max cloudcover
        .map(getBandsL457);

//combine all collections to one new collection
var composition = ee.ImageCollection(cL5.merge(cL4).merge(cL7).merge(newcL8))
var filteredLandsat = composition.select(['B2','B3','B4'], ['B2','B3','B4'])
        .median();

print('Result', filteredLandsat);
var visParams = {bands: ['B4', 'B3', 'B2'], min: 600, max: 2000};
Map.addLayer(filteredLandsat, visParams, 'Landsat');

//Classification
//Merge feature collections
var newfc = land.merge(water).merge(mudbank).merge(subtidal_mudbank);
print(newfc);

// Use these bands for classification.
var bands = ['B2', 'B3', 'B4'];
// The name of the property on the points storing the class label.
var classProperty = 'landcover';

// Sample the composite to generate training data.  Note that the
// class label is stored in the 'landcover' property.
var training = filteredLandsat.select(bands).sampleRegions({
  collection: newfc,
  properties: [classProperty],
  scale: 30
});

// Train a CART classifier.
var classifier = ee.Classifier.cart().train({
  features: training,
  classProperty: classProperty,
});
// Print some info about the classifier (specific to CART).
print('CART, explained', classifier.explain());

// Classify the composite.
var classified = filteredLandsat.classify(classifier);
Map.centerObject(newfc);
Map.addLayer(classified, {min: 0, max: 3, palette: ['green','blue', 'red', 'yellow']}, 'classification');

print('ResultClassification', classified)  ;
```

```
// To save the map results to your googledrive as geotiff
 Export.image.toDrive({
   image: classified,
  description: ['mudbanks_', yearStart, '-', yearEnd].join(''),
   crs: 'EPSG:4326',
   scale: 100,
   region: roi,
   maxPixels: 1500000000,
 });

 // To save the map results to your googledrive as geotiff
 Export.image.toDrive({
   image: filteredLandsat,
  description: ['Landsat_image_', yearStart, '-', yearEnd].join(''),
   crs: 'EPSG:4326',
   scale: 100,
   region: roi,
   maxPixels: 1500000000,
 });
```